Microbiome

RESEARCH

Open Access

Metabolome-driven microbiome assembly determining the health of ginger crop (*Zingiber officinale* L. Roscoe) against rhizome rot

Wenbo Wang[1], Nayanci Portal-Gonzalez[1], Xia Wang[1], Jialin Li[1], Hui Li[1], Roxana Portieles[2], Orlando Borras-Hidalgo[2], Wenxing He[1*] and Ramon Santos-Bermudez[1*]

Abstract

Background Plant-associated microorganisms can be found in various plant niches and collectively comprise the plant microbiome. The plant microbiome assemblages have been extensively studied, primarily in model species. However, a deep understanding of the microbiome assembly associated with plant health is still needed. Ginger rhizome rot has been variously attributed to multiple individual causal agents. Due to its global relevance, we used ginger and rhizome rot as a model to elucidate the metabolome-driven microbiome assembly associated with plant health.

Results Our study thoroughly examined the biodiversity of soilborne and endophytic microbiota in healthy and diseased ginger plants, highlighting the impact of bacterial and fungal microbes on plant health and the specific metabolites contributing to a healthy microbial community. Metabarcoding allowed for an in-depth analysis of the associated microbial community. Dominant genera represented each microbial taxon at the niche level. According to linear discriminant analysis effect size, bacterial species belonging to *Sphingomonas*, *Quadrisphaera*, *Methylobacterium-Methylorubrum*, *Bacillus*, as well as the fungal genera *Pseudaleuria*, *Lophotrichus*, *Pseudogymnoascus*, *Gymnoascus*, *Mortierella*, and *Eleutherascus* were associated with plant health. Bacterial dysbiosis related to rhizome rot was due to the relative enrichment of *Pectobacterium*, *Alcaligenes*, *Klebsiella*, and *Enterobacter*. Similarly, an imbalance in the fungal community was caused by the enrichment of *Gibellulopsis*, *Pyxidiophorales*, and *Plectosphaerella*. Untargeted metabolomics analysis revealed several metabolites that drive microbiome assembly closely related to plant health in diverse microbial niches. At the same time, 6-({[3,4-dihydroxy-4-(hydroxymethyl)oxolan-2-yl]oxy}methyl)oxane-2,3,4,5-tetrol was present at the level of the entire healthy ginger plant. Lipids and lipid-like molecules were the most significant proportion of highly abundant metabolites associated with ginger plant health versus rhizome rot disease.

Conclusions Our research significantly improves our understanding of metabolome-driven microbiome structure to address crop protection impacts. The microbiome assembly rather than a particular microbe's occurrence drove ginger plant health. Most microbial species and metabolites have yet to be previously identified in ginger plants. The indigenous microbial communities and metabolites described can support future strategies to induce plant disease resistance. They provide a foundation for further exploring pathogens, biocontrol agents, and plant growth promoters associated with economically important crops.

Keywords Microbiome, Metabolome, Microbial assembly, Ginger, Plant disease

*Correspondence:
Wenxing He
chm_hewx@ujn.edu.cn
Ramon Santos-Bermudez
bio_ramon@ujn.edu.cn
Full list of author information is available at the end of the article

Background

Plant-associated microorganisms can be found in various plant niches and collectively comprise the plant microbiome [1]. Plant microbiomes contain beneficial and pathogenic microbes [2]. Advances in high-throughput sequencing techniques have deepened our knowledge of the relationship between microbiomes and hosts [2].

Plant microbiome assemblages separated into above- and belowground constituent parts have been extensively studied, primarily in model species, including the soil microbiome [3–5], rhizosphere [6–10], root [11–13], and phyllosphere [14, 15]. Microbial communities associated with several plant niches have also been analyzed [16]. Fungus-induced changes are correlated with changes in the wheat leaf microbiome [17]. However, understanding the variation in the microbiome is imperative for determining how microbiome assembly affects overall plant holobiome health.

Conversely, plant secondary metabolites (PSMs) perform many functions, including defense against pathogens [18]. PSMs capable of broadly changing plant microbiomes have been described [2]. Phytohormones such as jasmonic acid (JA), salicylic acid (SA), ethylene (ET), and abscisic acid (ABA), among the most studied pathogenesis mediators, have also been shown to have an impact on the microbiome of plants [7, 11, 19].

The plant microbiome and metabolome are closely correlated, which indicates that endophytes can promote the accumulation of secondary metabolites that are relevant to active medicinal properties [20, 21]. The rhizosphere microbiome was shown to drive the systemically induced root exudation of metabolites [22]. Less attention has been given to the effects of the metabolome–microbiome relationship on plant health, although the interactive effect of host plant defense and root-associated microbiota is evident after *Fusarium oxysporum* infection in *Arabidopsis thaliana* [12].

Although little research has been conducted on ginger (*Zingiber officinale* L. Roscoe) compared to other agricultural plants [23], ginger is a perennial monocotyledonous herb with underground rhizomes and a long history of use as a fresh vegetable, spice, and herbal medicine. However, this crop is vulnerable to various plant pathogens [24], and rhizome rot has been a significant limiting factor for ginger's yield and marketing potential in China.

Rhizome rot is a highly destructive disease that has been found to reduce ginger production by 50–90% [25]. The disease causes significant losses, especially in warm and humid conditions, with severe outbreaks observed in recent years. In 2020, rhizome rot led to an average yield loss of 20 to 25% in the Tangshan region, posing a significant threat to local ginger farming [26]. This disease has increasingly become one of the most devastating issues for ginger cultivation in Shandong Province, a key ginger production area in China [27].

Further research on the disease's epidemiology and potential management options is necessary. Ginger rhizome rot can be attributed to multiple causal agents, including *Fusarium oxysporum* f. sp. *Zingiberi* [25], *Pectobacterium brasiliense* [26], *Bacillus pumilus* [27], *Pythium myriotylum* [28], and *Enterobacter cloacae* [29]. This complex pathosystem is worth studying to determine the microbiome and the metabolome assembly that keeps plants healthy. Here, we performed metataxonomic analyses using bacterial and fungal amplicon sequencing and untargeted metabolomics analysis to identify the metabolome-driven structure and function of microbial communities associated with rhizome rot and ginger plant health.

Methods

Sample collection and preparation

Samples were collected in the Laiwu district of Jinan, Shandong Province (1.36°19′50" N, 117°29′29" E; northern China), which has optimal growing conditions, but rhizome rot is a factor limiting the yield and marketability of ginger [28]. The sampling area is in a typical warm-temperate humid/semihumid climate zone, with an annual mean temperature of 12.5 °C, annual mean precipitation of 688.9 mm, and 62% relative humidity. The frost-free period is 191 days, and the annual sunshine hours are 2629 h [30]. Almost 70% of the total precipitation occurs from July to September. The soil in the area is classified as sandy loam [31].

The ginger variety used, *Zingiber officinale* var. officinale, was the same as that planted by local farmers. The size of each plot was approximately 666 m^2, and 7000 to 8000 plants were grown in each plot. The plots were subjected to the same irrigation and fertilization regimes. These plants were watered ten times during the crop growth cycle. Approximately 100 kg of compound and organic fertilizer (chicken manure) were applied to the soil at various times during the crop cycle, including during soil preparation, sowing, and crop growth. Sample collection was performed on September 12, 2021. In September, the mean temperature is 25°C during the day and 18°C at night. The relative humidity of the soil is 75–85%, and the area is exposed to 9 h of sunshine on average. Only ginger was grown within a radius of at least 1500 m in the sampled area. The area where samples are collected is also utilized for planting garlic. The crop rotation cycle occurs every 2 years, and this area has been dedicated to ginger farming for approximately 40 years. The diseased plants were stunted with yellowish, dry lower leaves that turned brown. Additionally, their rhizomes

were rotted or spongy, which aligns with the symptoms of rhizome rot previously described [25]. Endophytic bacteria were identified from asymptomatic plant tissues, but there was a notable increase in P*ectobacterium_carotovorum*_subsp._*brasiliense* (Supplementary Table 1) in diseased plants compared to healthy plants. Three replicates of healthy and diseased plants were collected from three adjacent plots. Each replicate consisted of a composite sample obtained by mixing three samples collected from the same niche (leaf, stem, root, rhizome, rhizosphere soil, and bulk soil; Fig. 1D) from three symptomatic or asymptomatic plants per plot for a total of 36 composite samples. The rhizosphere is the microbial habitat around the root [32], although we also applied this term to the soil adjacent to the rhizome. Approximately 30 g of bulk soil sample was collected at a distance of 20 cm from the root and at a depth of 0 to 15 cm, and the rhizosphere soil attached to the roots and rhizomes was collected by manual shaking. The samples were subsequently transferred to collection bags and transported to the laboratory on dry ice. Plant samples were washed immediately upon arrival at the laboratory with tap water until they appeared to be free of debris and then rinsed three times with distilled water (dH_2O). To sterilize the surface of the plant organs and remove exogenous bacteria and fungi, the samples that were used for endophytic diversity analyses were immersed in 70% ethanol for 5 min, 2.5% sodium hypochlorite solution for 1–2 min, and 70% ethanol for 1 min and then rinsed vigorously three times with sterilized Millipore water. To verify the efficacy of the sterilization process, a sample from the last portion of the water used for washing was inoculated on potato dextrose agar (PDA) plates, which were incubated at 28 °C for 10 days, and on LB plates, which were incubated at 37 °C for 5 days before checking for the appearance of colonies [33]. The surface-sterilized plant organs constituted the endophyte samples. Samples for molecular analysis were stored in a − 80°C freezer until DNA extraction.

DNA extraction and PCR amplification

All laboratory protocols were performed at Shanghai Majorbio Bio-pharm Technology Co., Ltd. The samples were processed under normal experimental conditions. Illumina metagenomic library preparation guidelines were followed to create 16S and ITS rRNA gene amplicon libraries. DNA extraction from 0.5 g of rhizosphere and bulk soil samples or 5 g of plant tissues was performed using a DNeasy PowerSoil Kit (Qiagen, MD, USA) according to the manufacturer's instructions. After the genomic DNA extraction was completed, 1% agarose gel electrophoresis was carried out to detect the extracted genomic DNA. DNA was quantified using a NanoDrop spectrophotometer. Each sample was tested three times and kept at − 20℃ until PCR amplification was performed. The V5–V7 hypervariable region of the bacterial 16S rRNA gene was amplified using the universal primers 799F (5′-AACMGGATTAGATACCCKG-3′) and 1193R (5′-ACGTCATCCCCACCTTCC-3′), which provided a more accurate picture of the bacterial community structure and very low amplification of nontarget DNA [10], while the fungal ITS2 region was amplified using the primers ITS3F (5′-GCATCGATGAAGAACGCAGC-3′) and ITS4R (5′-TCCTCCGCTTATTGATATGC-3′) [34], which proved to be the most appropriate for the characterization of fungal communities with metabarcoding [35]. An AxyPrep DNA Gel Recovery Kit (AXYGEN) was used to excise the products from the gel and recover them according to the manufacturer's instructions. PCR products were assessed and quantified with the QuantiFluorTM-ST Blue Fluorescence Quantitative System (Promega Corporation, Madison, WI, USA). Replicates of the same sample were pooled in equimolar proportions for sequencing.

Amplicon sequencing and bioinformatic analysis

The bacterial and fungal amplicon sequences of the 36 analyzed samples were independently sequenced. Negative controls were used (sterile water was used instead of template DNA) to exclude contamination by PCR amplification. Amplicon libraries were sequenced on the Illumina MiSeq PE300 platform (Illumina, USA) according to the manufacturer's protocols, and 250 bp paired-end reads were generated. The 16S rRNA and ITS gene sequences generated were analyzed using the online Majorbio Cloud Platform [36] based on the QIIME pipeline [37] version 1.9.1 using recommended parameters. Paired-end reads obtained from the Illumina platform were assembled, and the primer sequences and low-quality reads with scores less than Q30 were trimmed using USEARCH v.11.0 software [38] with default parameters. The sequencing run produced 2,645,244 high-quality reads across the 36 input libraries. Operational taxonomic units (OTUs) were assigned based on 97% similarity among clustered reads and then checked for chimeras using the UPARSE (v.7.0.1090, https://drive5.com/uparse/) pipeline [39] in USEARCH v.11.0 software [38] with default parameters before generating an OTU count table. OTUs were taxonomically annotated using the SILVA reference database (v.138, https://www.arb-silva.de) and I database (v.8.0, http://unite.ut.ee/index.php) for bacteria and fungi, respectively. The Shannon rarefaction curve was calculated (Supplementary Fig. 1A and 1B) by randomly resampling each sample several times, plotting the rarefied number of OTUs defined at a 97% sequence similarity threshold

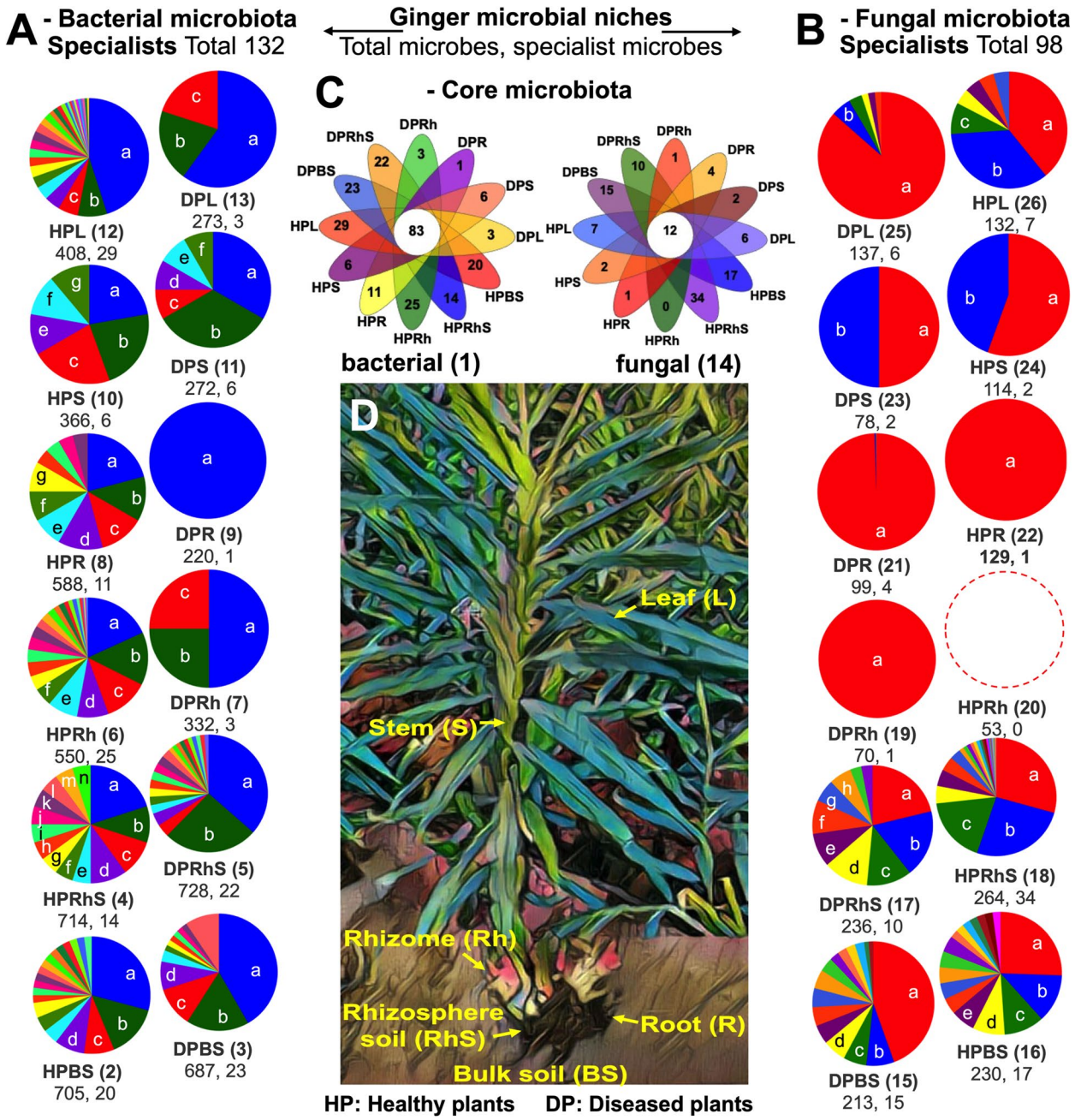

Fig. 1 The plant disease rhizome rot drives changes in the assembly of the microbiota associated with the entire ginger plant. Occurrence of specialist bacterial (**A**) and fungal (**B**) genera in healthy and diseased ginger plant niches. **C** Number of core/specialists bacterial and fungal microbes. **D** Sampling diagram of various ginger microbial niches. Each pie chart shows the number of specialist microbes inhabiting a specific microbial niche, and the most abundant microbes (> 5%) per niche are indicated by letters. The microbial niches are numbered beside each one, and the specialist microbes per niche are listed in Supplementary Table 3. The numbers shown below each abbreviation equal the total number of microbes and the number of specialist microbes for each microbial niche. An empty circle is shown for HPRh, indicating the absence of specialist microbes inhabiting that microbial niche. HPBS healthy plant bulk soil, DPBS diseased plant bulk soil, HPRhS healthy plant rhizosphere soil, DPRhS diseased plant rhizosphere soil, HPRh healthy plant rhizome, DPRh diseased plant rhizome, HPR healthy plant root, DPR diseased plant root, HPS healthy plant stem, DPS diseased plant stem, HPL healthy plant leaf, DPL diseased plant leaf

relative to the number of samples (Mothur v.1.30.2, https://www.mothur.org/wiki/Download_mothur), and the minimum number required for subsequent analysis was validated. We performed a single rarefaction at a depth of the shallowest sample to control for variable sequencing effort between representatives. Then, we chose a subsampling depth of 27,618 sequences per bacterial sample and 45,861 per fungal sample, which yielded a final rarefied dataset for all 36 models. Bacterial and fungal sequences were assigned to each sample based on their barcodes using the SILVA v138 16S (http://www.arb-silva.de) and UNITE v8.0 ITS (http://unite.ut.ee/index.php) databases, respectively.

Microbial diversity analysis

Although different indices showed very similar results (source data Fig. 2), plant health was related to both diversity and microbial composition [40]. Thus, two alpha diversity indices were considered at the genus level: observed richness (Sobs), which provides a direct measure of population complexity by counting the number of different species in a sample (observed OTUs), and the Shannon H' index, which is an estimator of taxon diversity, combining richness, and uniformity [41] with the Kruskal–Wallis test for all pairwise combinations. Principal coordinate analysis (PCoA) was conducted with the vegan package v.2.4.3 in R software v.3.3. [42] based on the Bray–Curtis distance algorithm to visualize the β diversity pattern of microbial communities between samples from different microbial niches of healthy and diseased plants. Permutational multivariate analysis of variance (PERMANOVA) was performed using 999 permutations computed from the rarefied dataset ($n=36$) to test the relative contribution of both disease and plant compartment microhabitats to community dissimilarity. The core or generalist taxa in the ginger microbiomes were defined as OTUs present in 100% of the plant samples, while the specialists were present in only one plant niche.

Predictive and statistical analysis

The data are displayed as the average of at least three independent replications and the standard deviation. *P* values less than 0.05 were considered to indicate statistical significance. We summarized the distribution of the annotated OTUs based on the species results to reveal the general species distribution patterns of the different samples. In particular, pie diagrams were generated to indicate the numbers of shared (core) or unique (specialist) microbial genera among compartments for healthy and diseased ginger plants. Clustering heatmaps reflecting differences in the abundance of different samples through color changes were generated (ggplot2' package v3.2.1 in R Studio v3.5.3). Microbial functional assemblages from 16S rRNA gene sequences were predicted by FAPROTAX [43] and were compared using the Kruskal–Wallis rank sum test, while fungal OTUs were classified into ecological guilds using the online application FUNGuild [44]. A confidence ranking of "highly probable" or "probable" was retained for high accuracy, whereas those with "possible" confidence rankings were considered unclassified. Undefined guilds: undefined pathogens, defined as nonspecific pathogens of fungi, plants, or animals; undefined saprotrophs, defined as nonspecific saprotrophs of wood, plants, or litter soil. Linear discriminant analysis (LDA) effect size (LEfSe) was applied to determine the features (differentially enriched microbial taxa and functions) most likely to explain differences between healthy and diseased ginger plants. The samples were pooled to analyze the soil and endophyte microbiomes of plants that appeared healthy or diseased. Taxa with an LDA effect size greater than 4.0 ($P<0.05$) were considered significant.

Metabolomics analysis

We analyzed changes in the endophyte microbiome of plants driven by the metabolome and implications for plant health. The same 24 samples of leaves, stems, roots, and rhizomes from healthy and diseased plants that were used for the microbiome analysis were analyzed using an untargeted metabolomics approach. Fifty milligrams of each sample was added to a 2-ml centrifuge tube, and a 6-mm diameter grinding bead was added. For the extraction of the metabolite, 400 μL of methanol:water (4:1 (v:v)) containing 0.02 mg/mL internal standard (L-2-chlorophenylalanine) was used. The samples were ground with a Wonbio-96c frozen tissue grinder (Shanghai Wanbo Biotechnology Co., Ltd.) for 6 min (−10°C, 50 Hz), followed by ultrasonic extraction at a low temperature for 30 min (5°C, 40 kHz). The samples were kept at −20°C for 30 min and then centrifuged for 15 min (4°C, 13,000*g*), after which the supernatant was transferred to an injection vial for LC–MS/MS analysis in positive and negative ionization modes. A pooled quality control sample (QC) was prepared by mixing equal volumes of all the samples. The QC samples were disposed and tested in the same manner as the analytic samples. LC–MS/MS analysis of the samples was conducted on a SCIEX UPLC-Triple TOF 5600 system equipped with an ACQUITY HSS T3 column (100 mm × 2.1 mm i.d., 1.8 μm; Waters, USA) at Majorbio Bio-Pharm Technology Co., Ltd. (Shanghai, China). The mobile phases consisted of 0.1% formic acid in water:acetonitrile (95:5, v/v) (solvent A) and 0.1% formic acid in acetonitrile:isopropanol:water (47.5:47.5, v/v) (solvent B). The flow rate was 0.40 mL/min, and the column temperature was 40°C. The UPLC system

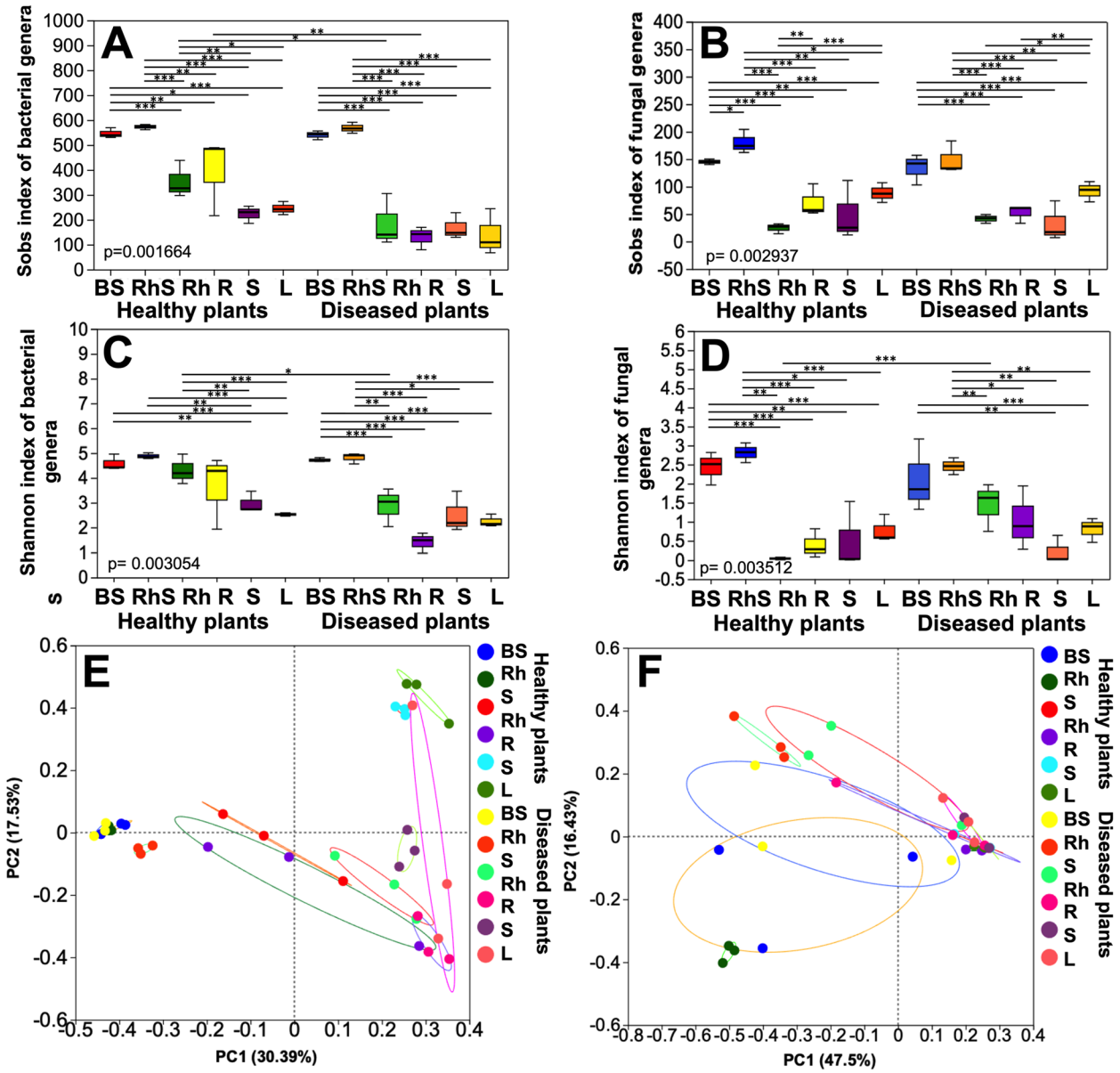

Fig. 2 Diversity analysis at the genus level for microbial communities from the niches of healthy and diseased ginger plants. Box plots of alpha diversity showing the Sobs index (**A**) and Shannon index (**C**) for archaeal/bacterial communities at the genus level and the Sobs index (**B**) and Shannon index (**D**) for fungal communities at the genus level for both healthy and diseased ginger plants. The bars represent the average of three composite biological replicates for each microbial niche, and the error bars indicate the standard variation in the mean. Significance was tested using a Kruskal–Wallis rank sum test; $^{*}P < 0.05$, $^{**}P < 0.01$, $^{***}P < 0.001$. Principal coordinate analysis (PCoA) plot visualizing variation in the bacterial (**E**) and fungal (**F**) community compositions of healthy and diseased plant samples in two-dimensional space based on Bray–Curtis dissimilarity. Permutational multivariate analysis of variance (PERMANOVA) by Adonis was performed to test the significance of microbial community dissimilarity. Each dot represents a single composite sample. Lines are drawn to connect three replicates of each composite sample to each other. The different colors in the figure represent different microbial niches

was coupled to a quadrupole time-of-flight mass spectrometer (Triple TOFTM5600^{+}, Sciex, USA) equipped with an electrospray ionization (ESI) source operating in positive mode and negative mode. The optimal conditions were set as follows: source temperature, 550°C; curtain gas (CUR), 30 psi; Ion Source Gas1 and Gas2, 50 psi; ion-spray voltage floating (ISVF), −4000 V in negative mode and 5000 V in positive mode; declustering potential, 80 V; collision energy (CE); and 20–60 eV rolling for MS/MS. Data acquisition was performed in

information-dependent acquisition (IDA) mode. Detection was carried out over a mass range of 50–1000 m/z. Pretreatment of the raw LC/MS data was performed with Progenesis QI (Waters Corporation, Milford, USA) software, and a three-dimensional data matrix was exported in CSV format. Internal standard peaks, as well as any known false-positive peaks (including noise, column bleeding, and derivatized reagent peaks), were removed from the data matrix, and the peaks were pooled. Moreover, the metabolites were identified by searching databases, and the main databases used were the HMDB (http://www.hmdb.ca/), Metlin (https://metlin.scripps.edu/), and Majorbio databases. The data were analyzed through the free online platform Majorbio cloud (cloud.majorbio.com). At least 80% of the metabolic features detected in any set of samples were retained. To reduce the errors caused by sample preparation and instrument instability, the response intensity of the sample mass spectrum peaks was normalized by the sum normalization method, after which the normalized data matrix was obtained. The RSD was less than 0.3 for the overall dataset, and the peak ratio was more than 70%, so the overall data were suitable for subsequent analysis (Supplementary Fig. 3). The total set of metabolites identified was annotated using public databases, including KEGG (Kyoto Encyclopedia of Genes and Genomics, http://www.genome.jp/kegg/) and HMDB (Human Metabolome Database, www.hmdb.ca). Pearson's correlation based on the Bray–Curtis distance algorithm was used to evaluate the abundance of endophyte microbiome at the genus level and metabolites in the ginger plant compartments. Correlation analysis heatmaps were drawn, and KEGG enrichment analysis of the differentially abundant metabolites was performed using SciPy v.1.0.0 (Python) software. The differentially abundant metabolites were screened with the orthogonal projections to latent structures discriminant analysis (PLS-DA) model using the default criteria, with a variable importance value (VIP) ≥ 1 and a significance threshold of $P < 0.001$, using ropls v.1.6.2 (R software). Procrustes analysis of the Euclidian distances of eigenvalues for both the bacterial or fungal microbiome and metabolome datasets was executed to analyze the congruence of two-dimensional shapes produced from the superimposition of principal component analyses (PCAs) [45].

Results

Overview of the sequencing and de novo assembly

Data analysis of 36 composite samples from 6 microbial niches of healthy and diseased plants was carried out to characterize the microbial communities associated with the sampled ginger plants. Supervised taxonomic classification of all high-quality reads was performed using the SILVA and UNITE databases to examine the taxonomic structure of the bacterial and fungal communities, respectively. A total of 994,248 archaeal/bacterial and 1,650,996 fungal high-quality reads were obtained and sorted into 5353 archaeal/bacterial and 1793 fungal operational taxonomic units (OTUs). Archaeal/bacterial OTUs were assigned to 2 domains, 2 kingdoms, 44 phyla, 125 classes, 304 orders, 517 families, 1073 genera, and 2101 species (Supplementary Table 1), and the fungal OTUs were assigned to 15 phyla, 51 classes, 112 orders, 233 families, 426 genera, and 667 species (Supplementary Table 2). The saturated rarefaction curves (Supplementary Fig. 1A, B) and species diversity (Shannon index) for both the archaeal/bacterial (Supplementary Fig. 1C) and fungal communities (Supplementary Fig. 1D) indicated that the sampling efforts were adequate to reflect the microbial communities within each sample. *Proteobacteria* (57.40%), *Actinobacteriota* (16.74%), *Bacteroidota* (8.24%), and *Firmicutes* (6.83%) were the dominant bacterial phyla, while unclassified_k_Fungi (62.08%) and *Ascomycota* (32.53%) were the dominant fungal phyla.

Despite the great diversity, the ginger ecosystem's bacterial and especially fungal communities were dominated by a few phyla among all samples, and we next examined how differences in the microbiome assembly can impact plant health.

Assemblage of plant-associated bacterial and fungal microbiota

Microbial composition in plant niches associated with plant health

To determine the microbial composition and relative abundance in the niches of healthy and diseased plants, we constructed pie diagrams to represent the number of generalist (shared) and specialist (inhabitants of a single niche) microbes between the niches of all the plants. The total number of microbes per niche included generalists, specialists, and those inhabiting more than one niche, known as satellites. A greater number of bacterial genera was found in the microbial communities of healthy plants compared to diseased plants, except in the rhizosphere soil, where the number of bacterial genera was higher in the diseased plants. A total of 3331 bacterial genera were identified in the healthy plants, with 138 unique to that group. In contrast, 2512 genera were detected in the diseased plants, with 58 unique to that group (Fig. 1). Only two representatives of archaeal microorganisms (g_norank_f_*Nitrososphaeraceae* and g_*Candidatus_nitrocosmicus*) were present in the analyzed soil samples analyzed, and their relative abundances were very low to be included in further analyses.

Eighty-three bacterial genera were identified as members of the core (generalist) bacterial microbiota (Fig. 1C,

Supplementary Table 3). The most abundant bacterial genera were *Flavobacterium* (10.48%), *Acidovorax* (8.78%), *Sphingomonas* (7.92%), *Methylobacterium-Methylorubrum* (6.38%), and *Bacillus* (5.07%). Compared with the same niches in the diseased plants, all the organs of the healthy plants except for the stem harbored the largest number of endophyte bacteria (total; specialist); this trend was more notable in the leaves and rhizomes than in the other organs (Fig. 1A).

Healthy plants' roots (588; 11) and rhizomes (550; 25) harbored the most significant number of endophyte bacterial genera. However, rhizome rot strongly reduced the number of these in the roots (220; 1) and rhizomes (332; 3). Diseased plants exhibited fewer specialist bacteria in all plant organs except the stems.

The most abundant fungal generalist genera were unclassified_k_Fungi (85.89%) and *Gibellulopsis* (5.20%) (Supplementary Table 3). The greatest number of fungal genera (total; specialist) was detected in the niches of healthy plants (922; 61) compared with diseased plants (833; 38) so the presence of the specialists was noticeably more affected by the disease. A greater abundance of fungal genera was observed in the rhizomes of diseased plants (70; 1) than in those of healthy plants (53; 0) (Fig. 1B).

Most of the taxa with relatively high abundances inside the diseased ginger plants were also detected in the soil, indicating that these taxa might have colonized the plants from the ground. Interestingly, the rhizomes of the diseased plants harbored a greater diversity of fungi than did those of the healthy plants, while the opposite occurred for bacteria.

Rhizome rot drives microbial community assembly in diverse plant niches

To quantify the diversity and summarize the structural changes in the microbial community, we first used the Kruskal–Wallis test to calculate the microbial alpha diversity across all niches of healthy and diseased plants. The soil samples showed the highest diversity of bacteria (Fig. 2A, C) and fungi (Fig. 2B, D). The microbial communities in the rhizosphere were similar to those in the bulk soil, except for the fungal community in healthy plants, which was notably richer in the rhizosphere (Sobs index: 180 ± 21.6). Significant differences were observed in the bacteria and fungal populations among healthy plants.

The disease significantly reduced bacterial richness in both roots (healthy, 396.3 ± 56.2; diseased, 130.0 ± 26.2; $P = 0.0439$) and rhizomes (healthy, 353.7 ± 44.5; diseased, 185.0 ± 35.0; $P = 0.0431$) (Fig. 2A). Healthy plants had higher bacterial diversity in rhizomes (Shannon H': 4.30 ± 0.6). Diseased plants showed significant differences in fungal richness (Sobs index: 24.33 ± 9.3, Fig. 2B) and diversity (Shannon H': 0.04 ± 0.0, Fig. 2D) in rhizomes compared to healthy plants.

To assess the microbial community dissimilarity between the niches of healthy and diseased plants, principal coordinate analysis (PCoA) based on Bray–Curtis distance was performed (Fig. 2E, F). The closer the distance between samples in the PCoA diagram, the more similar their community composition. The analysis revealed differences in bacterial and fungal microbiome compositions between healthy and diseased plants. The first two axes account for about 50% and 47.5% of the variation for bacterial microbiomes (PERMANOVA, $R = 0.70$, $P < 0.001$; ANOSIM: $R = 0.73$, $P < 0.001$) and fungal microbiomes (PERMANOVA: $R2 = 0.63$, $P < 0.001$; ANOSIM: $R = 0.39$, $P < 0.001$), respectively. Different plant niches displayed distinct microbial communities, suggesting a potential link to plant health. These findings indicate that plant health is connected to unique microbial communities in various parts of the plant.

Additionally, functional signatures related to plant health status were predicted via FAPROTAX analysis based on the classification results from 16S amplicon sequencing. Testing for significance was performed using a Kruskal–Wallis rank sum test (Fig. 3A, Supplementary Table 4). The analysis predicted that the bacteria inhabiting the stems of diseased plants would have the highest functional potential for nitrogen (9.29 ± 2.19%), nitrate (8.05 ± 3.70%), and nitrite (8.79 ± 2.28%) respiration; nitrite (7.55 ± 1.85%) and nitrate (7.55 ± 1.55%) ammonification; nitrate reduction (10.47 ± 4.16%); and plant pathogens (8.37 ± 2.04%), presumably associated with the highest relative abundance of *Pectobacterium* (Fig. 3B).

The most common functional groups of fungi were undefined saprotrophs in the bulk (25.19 ± 2.21%) and rhizosphere (37.09 ± 2.90%) soils of healthy plants, while in the diseased plants, these functional groups were dominant in the bulk soil (13.91 ± 1.03%), roots (18.12 ± 1.92%), and rhizomes (17.12 ± 1.28%). Interestingly, the highest levels associated with the ecological guild of plant pathogens were observed in the rhizosphere (27.75 ± 2.08%) and rhizomes (27.75 ± 2.19%) of diseased plants (Fig. 3C), associated with an increased relative abundance of various potential pathogens in these microbial niches (Fig. 3D, Supplementary Table 5).

The alpha diversity analysis indicates that plant roots and rhizomes harbor a significant number and variety of bacterial microbes. However, the presence of rhizome rot disease reduced these indices. In contrast, plant disease increased the diversity of the fungal microbes. Beta diversity analysis revealed changes in the composition of microbial communities in rhizosphere soil due to plant disease. Additionally, the composition of the bacterial microbiome in rhizomes and roots differed from that in

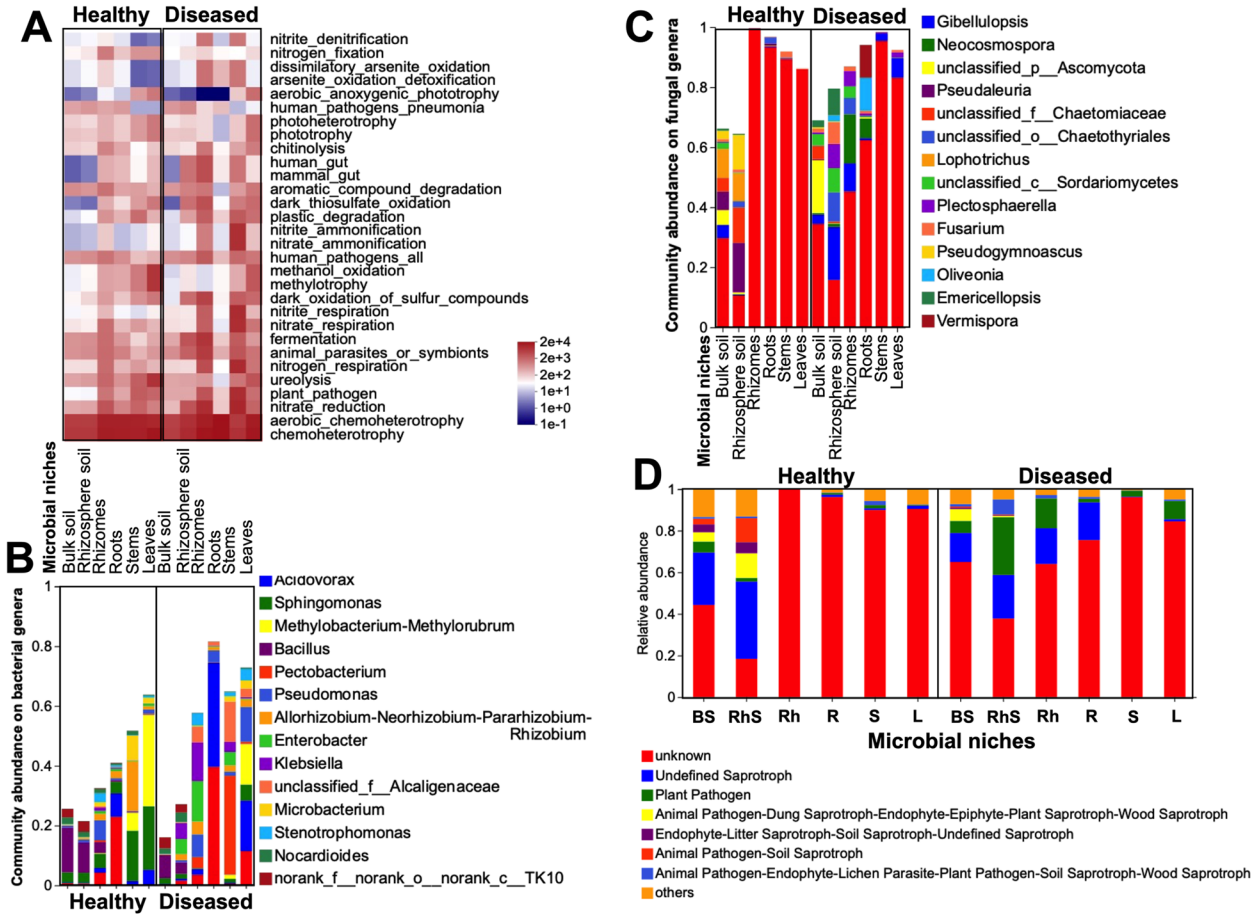

Fig. 3 Functional analysis of the bacterial and fungal genera from the various niches of healthy and diseased ginger plants. Genus-level distribution of the bacterial (**A**) and fungal (**C**) microbiome associated with different ginger plant niches. The length of the bars represents the percentage of each microbial genus per sample. Top genera with an abundance > 1% in at least one sample are shown. Clustered heatmap of top thirty predicted bacterial functional profiles (**B**). The samples are grouped according to their similarity to each other, and the clustering results are arranged horizontally according to the clustering results. The color bar indicates the relative abundance of microbial functions from lowest (blue) to highest (red). Variations in the composition of the top fungal functional groups (> 5%) inferred by FUNGuild analysis (**D**). BS bulk soil, RhS rhizosphere soil, Rh rhizome, R root, S stem, and L leaf

stems and leaves in healthy plants, but the disease nullified this difference.

Bacterial and fungal taxa potentially involved in plant health

We used linear discriminant analysis (LDA) effect size (LEfSe) to identify discriminative features at taxonomic levels for overall plant health regardless of the microbial niche. This study focused on potentially pathogenic and disease-suppressive microbes in soil and endophytes in plant tissues. In total, 105 taxa (from phylum to species) were identified with a log10 (LDA) score > 4.0 and a *P* value < 0.05.

In the LEfSe analysis, we found seven plant-endophyte bacteria (Fig. 4A) and five soilborne bacteria (Fig. 4B) that are biomarkers for plant health. Specifically, we observed that bacteria such as s_unclassified_g_*Sphingomonas*, *Quadrisphaera granulorum*, and *Methylobacterium komagatae* were significantly enriched in healthy plants. On the other hand, bacteria like *P. carotovorum* subsp. *brasiliense*, s_unclassified_f_Alcaligenaceae, *Alcaligenes faecalis*, and *Klebsiella aerogenes* were found to be significantly increased in diseased plants. Additionally, we found certain bacteria enriched in the soil of healthy and diseased plants.

Four species of endophyte plant fungi (Fig. 5A) and ten soil-borne fungi (Fig. 5B) were identified as potential biomarkers. In healthy plants, s_unclassified_k_Fungi (from phylum to species) was significantly enriched. Biomarkers associated with s_unclassified_g_*Cheilymenia* (from class to species), *Pseudaleuria* sp. (from genus

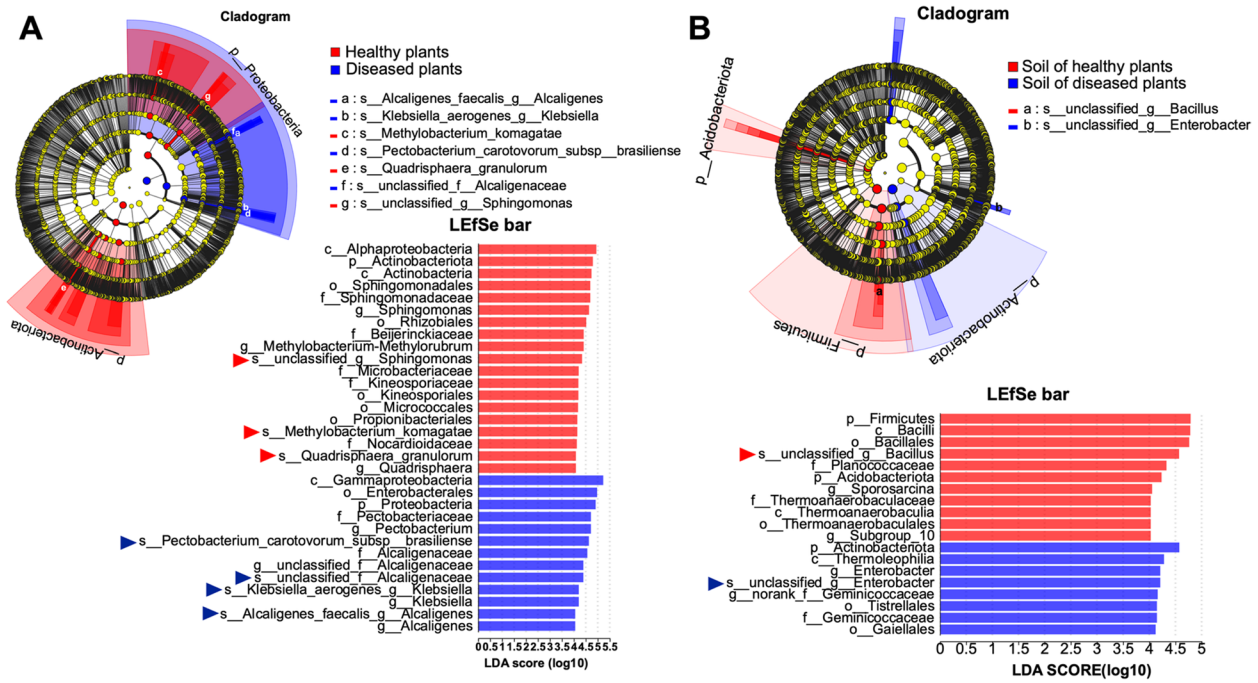

Fig. 4 LEfSe (LDA effect size) multilevel species hierarchy tree diagram (cladogram) and latent Dirichlet allocation (LDA) discrimination results diagram for endophytic (**A**) and soilborne (**B**) bacterial community biomarkers for plant health. The cladogram demonstrates the classification of taxa at the five levels, and the different colors indicate the differences in relative abundance for microbes that inhabit healthy (red) or diseased (blue) plants. Nonsignificant differences are represented by yellow circles. The LEfSe bar chart shows the biomarkers with significant differences between healthy and diseased plants, and the lengths of the bars indicate the influence of the species. The LDA score threshold was log10 (LDA score) > 4.0. The higher the LDA score is, the greater the impact of species abundance on the difference effect

to species), *Lophotrichus* sp. (order to species), *Pseudogymnoascus* sp. (from class to species), *Gymnoascus* sp. (order to species), *Mortierella polycephala* (phylum to species), and *Eleutherascus cristatus* (from family to species) were significantly increased in the soil of healthy plants. In diseased plants, *Gibellulopsis piscis* (from phylum to species), *Pyxidiophorales* sp. (from class to species), and *Plectosphaerella cucumerina* (from phylum to species) were enriched, serving as potential biomarkers of disease. However, only three fungal biomarkers were characteristic of the soil of diseased plants: *P. cucumerina* (from genus to species), *Trichoderm longibrachiatum* (species), and *Fusarium nematophilum* (species).

A probabilistic graph model related to a co-occurrence Bayesian network model (Supplementary Fig. 2A and B) shows a robust core bacterial and fungal microbiota and biomarkers linked to ginger plant health, including identifying *Pectobacterium* associated with rhizome rot in ginger plants. A greater network complexity has been associated with microbial communities exhibiting more intense activity and higher resilience to perturbation [16]. Our analysis of intrakingdom networks revealed a higher network complexity associated with increased nodes and edges in the bacterial networks (Supplementary Fig. 2B and C) than in the fungal networks (Supplementary Fig. 2D and E). The node average degree (206.48) and positive edges (48,524) were higher in the bacterial co-occurrence network in diseased plants than the node average degree (106.67) and positive edges (24,449) in healthy plants. However, the bacterial community in healthy plants had much higher opposing edges (1458) than in diseased ones (206). For fungal networks, the node average degree (35.97), positive edges (6,487), and opposing edges (23) were all higher in the healthy plants related to the node average degree (29.64), positive edges (4,816), and opposing edges (cero) in diseased plants.

Network statistics can determine the importance of microorganisms in co-occurrence networks [46]; in a co-occurrence network, hub or keystone species can be inferred by identifying species with the highest network centrality indices. The network analysis revealed that all bacterial biomarkers were highly prevalent in the system. *Bacillus* and *Sphingomonas* were identified as the most crucial nodes in the genus-level network within the healthy ginger ecosystem (Supplementary Table 6). The co-occurrence network for diseased plants revealed significant bacterial biomarkers. However, the ginger pathogen *Pectobacterium* [26] was identified as the top-ranking

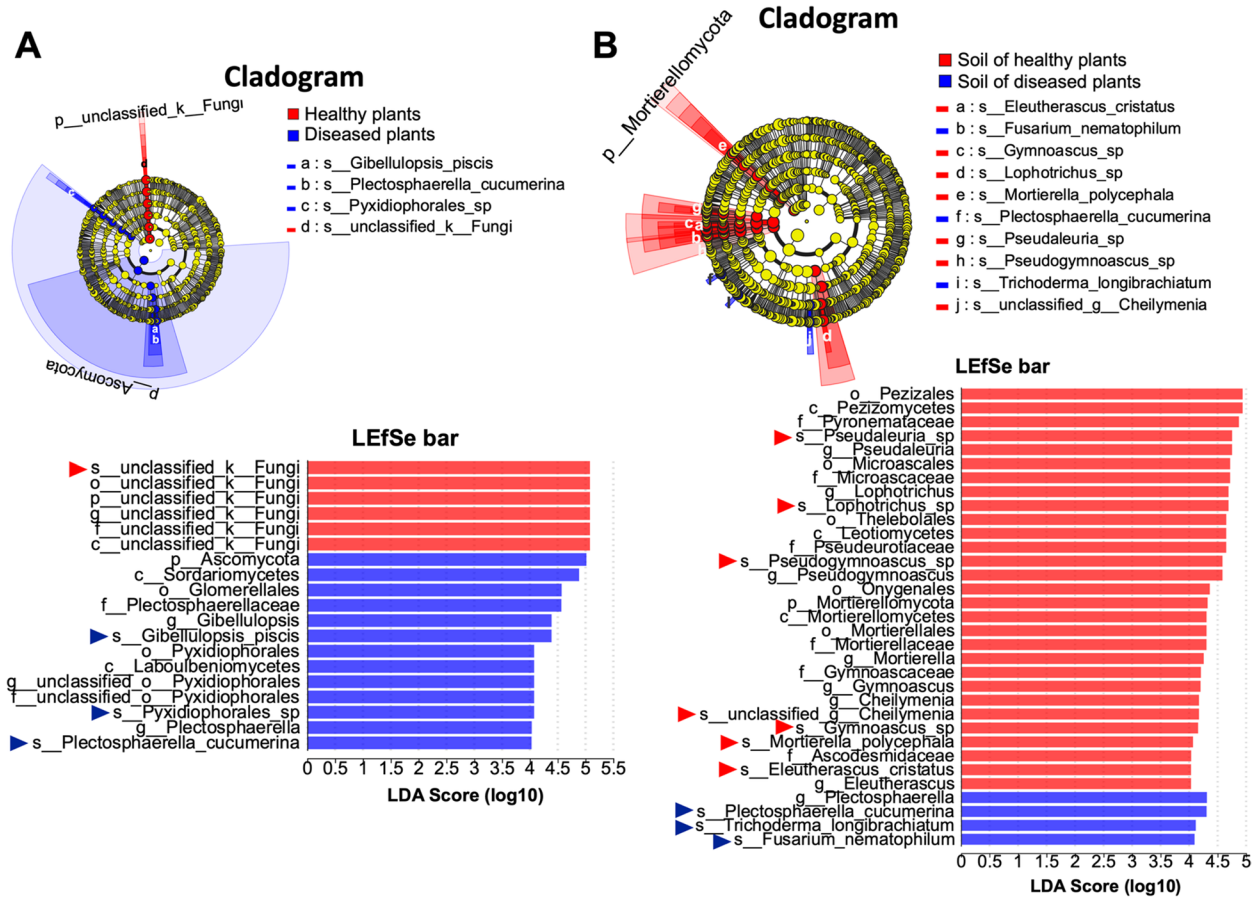

Fig. 5 Fungal biomarkers for plant health based on the LEfSe (LDA effect size) multilevel species hierarchy tree diagram (cladogram) and latent Dirichlet allocation (LDA) discrimination results diagram for endophytic (**A**) and soilborne (**B**) microbes. The cladogram demonstrates the classification of taxa at the five level, and the different colors indicate the differences in relative abundance for microbes that inhabit healthy (red) or diseased (blue) plants. Nonsignificant differences are represented by yellow circles. The LEfSe bar chart shows the biomarkers with significant differences between healthy and diseased plants, and the lengths of the bars indicate the influence of the species. The LDA score threshold was log10 (LDA score) > 4.0. The higher the LDA score is, the greater the impact of species abundance on the difference effect

bacterium (Supplementary Table 7). Moreover, the fungal biomarker exhibited a significant correlation within the microbial co-occurrence network of healthy ginger plants. Notably, *Pseudaleuria* and *Mortierella* emerged as prominent nodes with high degrees within the top 10 hub nodes (Supplementary Table 8). Conversely, the fungal networks of diseased plants featured *Plectosphaerella* and *Gibellulopsis* (Supplementary Table 9). These results emphasize the potential significance of these microbial strains in preserving the health of ginger plants.

Metabolites driving ginger microbial community assembly and plant health

Overview of metabolite information

We used untargeted metabolomics to simultaneously detect and analyze small-molecule metabolites that impact microbiome assembly and the health of ginger plants. The metabolomes of the niches corresponding to the vegetative organs of healthy and diseased plants were analyzed via LC–MS/MS, which revealed a total of 10,415 chromatographic peaks with 735 metabolites, 500 of which were in the library (annotated to public databases like HMDB and Lipidmaps), and 199 of which were annotated to the KEGG database (Table 1, Supplementary Table 10).

The metabolites identified across all the samples included 170 lipids and lipid-like molecules, 79 organic acids and derivatives, 63 organic oxygen compounds, and other compounds (Fig. 6A). The highest numbers of differentially accumulated metabolites (total; specific to each niche) were found in the rhizomes (164; 86), followed by the leaves (135; 63), roots (89; 35), and stems (76; 25). Interestingly, a metabolite associated with the health of the whole ginger plant (6-({[3,4-dihidroxi-4-(hidroximetil)oxolan-2-il]oxi}metil)oxano-2,3,4,5-tetrol) was identified (Fig. 6B).

Table 1 Total ion numbers and identification statistics

Ion mode	All peaks	Identified metabolites[a]	Metabolites in library	Metabolites in KEGG
Positive	4582	356	228	112
Negative	5833	379	272	87

[a] Annotated to public databases like HMDB and Lipidmaps

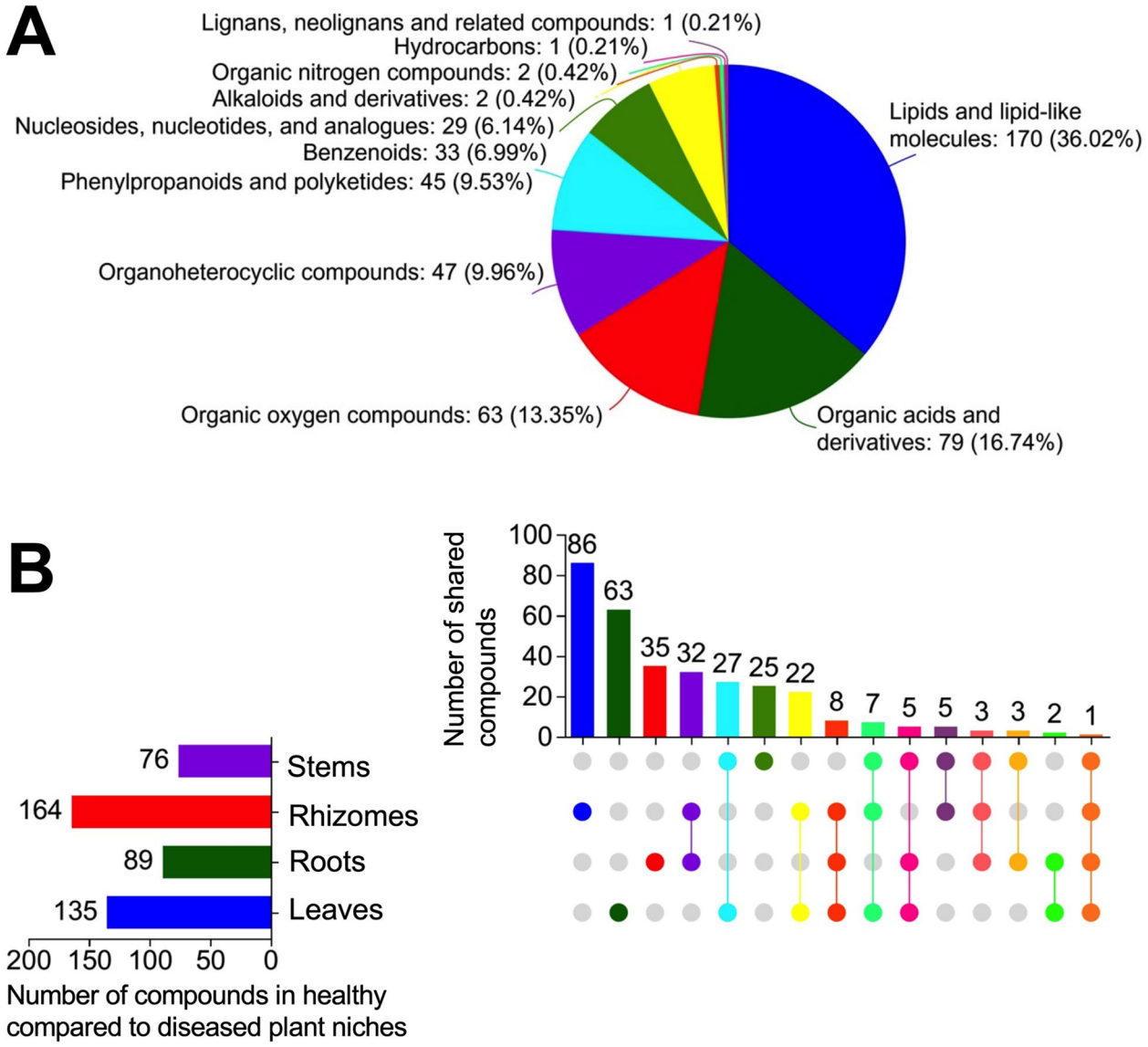

Fig. 6 Overview of metabolite information related to plant health. **A** Superclass classification of the main types of metabolites found in diverse organs of healthy and diseased plants. **B** Number of differentially accumulated metabolites in the microbial niches of healthy plant organs. The histogram in the lower left corner refers to the number of overexpressed compounds in each microbial niche. The bar graph on the right shows the number of compounds after the intersection of various metabolic sets belonging to microbial niches. The single point below represents specific metabolite within the metabolite set, and the connection between some points shows the number of common metabolites

The plant health-associated microbiome is driven by the metabolome

The relationship between plant health-associated microbes and metabolites was examined. Procrustes analyses were performed using distance plots (PCA) as input based on the matrix of endophytic microbial communities (Bray–Curtis). Significant associations were found between certain bacterial (M2 = 0.58, $P = 0.00$) and fungal (M2 = 0.84, $P = 0.04$) genera and metabolite synthesis. The associations varied based on plant health and microbial niches (Fig. 7A). In diseased plants, only fungi in the rhizomes and roots were closely linked to metabolite synthesis (Fig. 7B).

Furthermore, the metabolites that drive the assembly of the potentially plant health-determining microbiota according to the LEfSe analysis are detailed below. Similarly, trans-EKODE-(E)-Ib ($P = 0.0137$) and 2,3-dinor prostaglandin E1 ($P = 0.0359$) were positively related to *Sphingomonas*, while piperidine ($P = 0.0004$), cyclohexane ($P = 0.0006$), tripropylamine ($P = 0.0005$), palmitoleamide ($P = 0.0012$), farnesyl acetone ($P = 0.0031$), and C16 sphinganine ($P = 0.0055$) were negatively correlated with this bacterial genus. trans-EKODE-(E)-Ib ($P = 0.0341$) was positively related, while ethyl hydrogen sulfate ($P = 0.0008$), 2-dodecylbenzenesulfonic acid ($P = 0.0009$), piperidine ($P = 0.0034$), farnesyl acetone ($P = 0.0040$), 9,12,15-octadecatrien-1-ol ($P = 0.0042$),

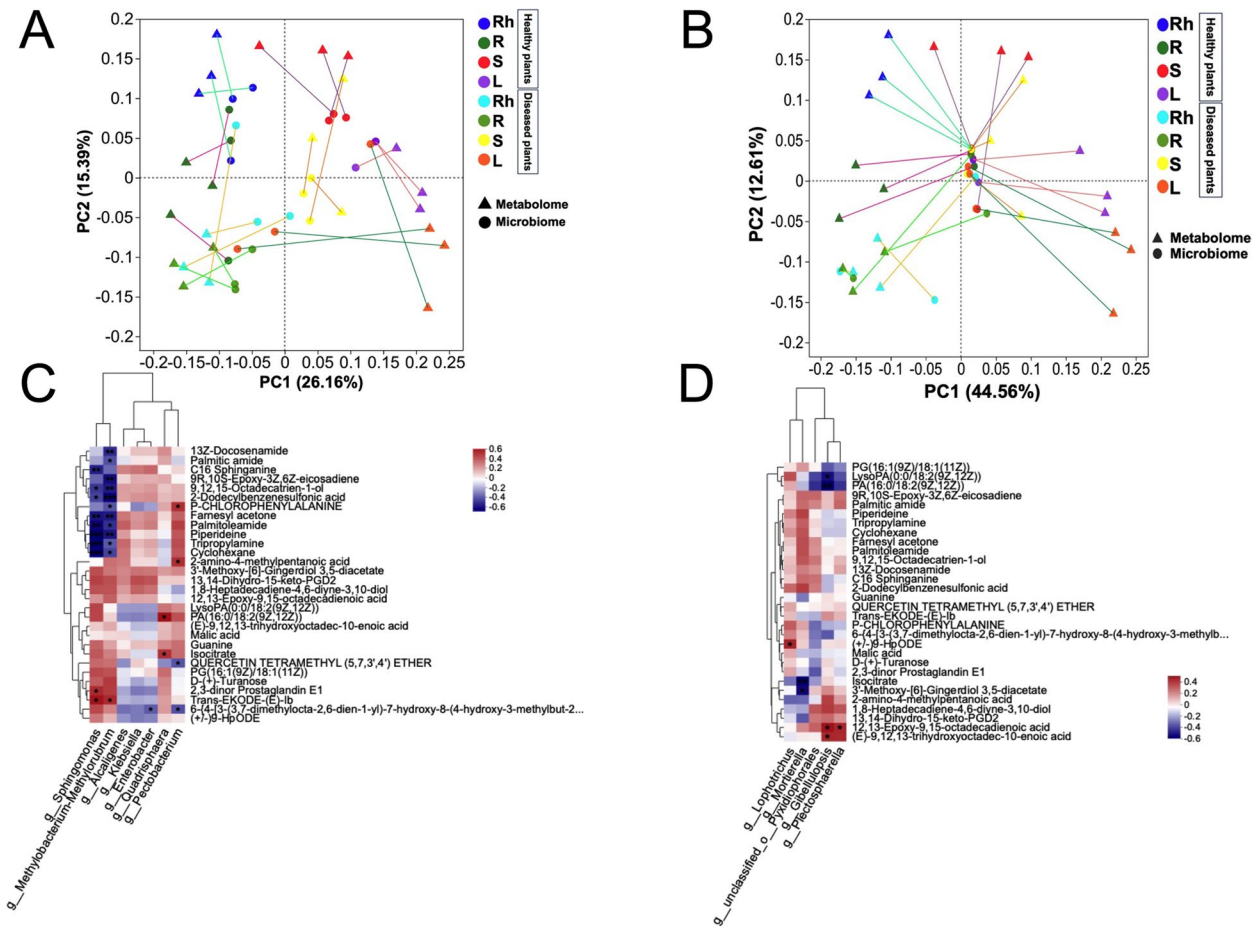

Fig. 7 Associations between the endophyte microbiota and the plant metabolome. Procrustes correlation between the metabolome and the endophyte bacterial (**A**) or fungal (**B**) microbiota. M2 represents the sum of squared distances between matched sample pairs; the lower the value is, the greater the correlation between the two sets of data. The Monte Carlo *P* value was determined from 999 labeled permutations and provides a general measure of consistency between the two datasets ($P < 0.01$ indicates that the composition of the microbial community and the expression of metabolites are very consistent; $P < 0.05$ indicates consistency between these two datasets; and $P > 0.05$ indicates that the trend of association between the datasets is not significant). The connection represents the Procrustes residue of the two ordered configurations, which can be used to assess the variation between the two. The longer the connection is, the lower the consistency between the two datasets. A heatmap based on Pearson's correlation indicated the associations between metabolites and bacterial (**C**) or fungal (**D**) communities at the genus level. Metabolites are shown on the right; microbial genera are shown at the bottom. Asterisks indicate Pearson's correlation coefficient (*$P < 0.05$; **$P < 0.01$; ***$P < 0.001$). The "blue to red" color gradient indicates the Pearson's correlation index value. A darker red color indicates a greater positive Pearson correlation coefficient, while a darker blue color indicates a greater negative correlation coefficient

13Z-docosenamide ($P=0.0090$), palmitoleamide ($P=0.0108$), cyclohexane ($P=0.0227$), palmitic amide (0.0358), p-chlorophenylalanine ($P=0.0424$), and tripropylamine ($P=0.0452$) were negatively correlated with *Methylobacterium–Methylorubrum*. Moreover, PA (16:0/18:2(9Z,12Z)) ($P=0.0120$) and isocitrate ($P=0.0482$) were positively related to *Quadrisphaera*. 2-Amino-4-methylpentanoic acid ($P=0.0421$) and p-chlorophenylalanine ($p=0.0449$) were positively related to *Pectobacterium*, while 6-{4-[3-(3,7-dimethylocta-2,6-dien-1-yl)-7-hydroxy-8-(4-hydroxy-3-methylbut-2-en-1-yl)-4-oxo-4H-chromen-2-yl]-3-hydroxyphenoxy}-3,4,5-trihydroxyoxane-2-carboxylic acid ($P=0.0364$) and quercetin tetramethyl (5,7,3',4') ether ($P=0.0379$) were negatively correlated with these bacteria. There was a significant positive correlation between linoleamide ($P=0.0185$) and *Alcaligenes*, and a negative correlation between this bacterial genus and DG (18:4 (6Z,9Z,12Z,15Z)/18:2 (9Z,12Z)/0:0) ($P=0.0086$) was detected. DG (18:4(6Z,9Z,12Z,15Z)/18:2(9Z,12Z)/0:0) was negatively correlated with *Klebsiella* ($P=0.005$). DG (18:4(6Z,9Z,12Z,15Z)/18:2(9Z,12Z)/0:0) ($P=0.005$) and 6-{4-[3-(3,7-dimethylocta-2,6-dien-1-yl)-7-hydroxy-8-(4-hydroxy-3-methylbut-2-en-1-yl)-4-oxo-4H-chromen-2-yl]-3-hydroxyphenoxy}-3,4,5-trihydroxyoxane-2-carboxylic acid ($P=0.0025$) were negatively correlated with *Enterobacter* (Fig. 7C).

12,13-Epoxy-9,15-octadecadienoic acid ($P=0.0235$), L-glutamate ($P=0.0353$), and (E)-9,12,13-trihydroxyoctadec-10-enoic acid ($P=0.0481$) were positively associated with *Gibellulopsis*, while PA(16:0/18:2(9Z,12Z)) ($P=0.0079$) and LysoPA(0:0/18:2(9Z,12Z)) ($P=0.0207$) were negatively related to this genus. 12,13-Epoxy-9,15-octadecadienoic acid ($P=0.0468$) was positively correlated with *Plectosphaerella*. (±)9-HpODE ($P=0.0428$) was positively correlated with *Lophotrichus*. Isocitrate ($P=0.0087$) and 3'-methoxy-[6]-gingerdiol 3,5-diacetate ($P=0.0167$) significantly affected the presence of *Mortierella* (Fig. 7D).

The metabolome can directly impact the health of ginger plants

To identify the compounds that play roles in plant health, the VIP combined with univariate statistical analysis was used. Of the total metabolites (anion plus cation), 470 (4.51%) were enriched and 711 (6.83%) were depleted in healthy ginger plants compared to diseased ginger plants (Fig. 8A). One hundred five annotated metabolites exhibited significant differences in abundance (Welch's two-sided *t* test, $P<0.05$) between the diseased and healthy ginger plants. In contrast, the abundances of 469 annotated metabolites were unchanged in either plant group (Fig. 8B). The abundance of 74 named metabolites was reduced, and 31 annotated metabolites were enriched in healthy plants compared to diseased plants. Particularly notorious, niacinamide, a heterocyclic aromatic amide ($P<0.001$), the metabolic intermediates involved in de novo lipid synthesis 1-oleoyl lysophosphatidic acid ($P<0.001$), and the phospholipid PG (16:0/16:0) ($P<0.05$) were enriched in healthy ginger plants, while the nonproteinogenic L-alpha-amino acid 4-methylene-L-glutamine, the alkaloid xanthine, and the purine derivative hypoxanthine, among others, were significantly more abundant ($P<0.001$) in diseased plants (Fig. 8C).

Metabolite profiles of plant niches revealed that niacinamide and PG (16:0/16:0) were upregulated in rhizomes (VIP value = 2.56, $P=0.0002$, and VIP value = 2.37, $P=0.0012$) and leaves (VIP value = 2.54, $P=0.0002$, and VIP value = 2.36, $P=0.0012$), while 1-oleoyl lysophosphatidic acid was upregulated in rhizomes (VIP value = 2.19, $P=0.0003$) and roots (VIP value = 2.19, $P=0.0003$) of healthy plants. In diseased plants, 4-methylene-L-glutamine was upregulated in leaves (VIP = 3.49, $P=0.0000$). Hypoxanthine and xanthine also were upregulated in leaves (VIP = 3.16, $P=0.0000$, and VIP = 3.29, $P=0.0000$), and the latter was also in rhizomes (VIP = 3.16, $P=0.0000$) (Supplementary Table 11).

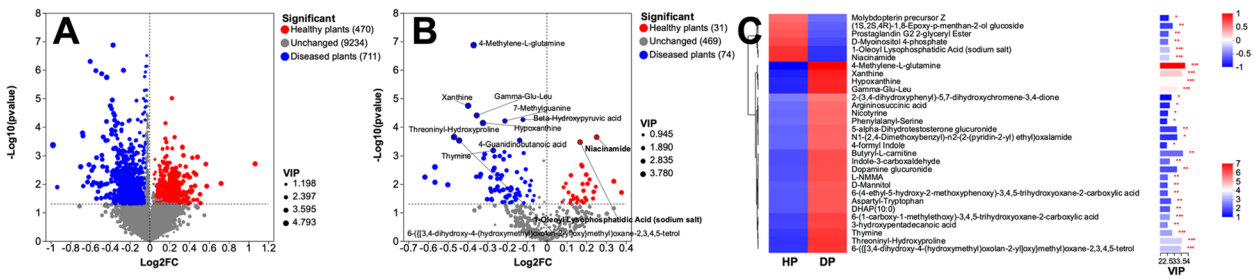

Fig. 8 Differences in the expression of all metabolites (**A**) and annotated metabolites (**B**) are associated with plant health. The first 12 metabolites in **B** are labeled according to the *P* value (Welch's two-sided *t* test). The values of the abscissa and ordinate are logarithmic. **C** The top 30 differentially expressed metabolites with variable importance in projection (VIP) values in the PLS-DA model for each group comparison. The columns represent samples from healthy (HP) and diseased (DP) plants, and each row represents a metabolite. The bar chart on the right shows the VIP scores of the metabolites. The length of each bar indicates the contribution of the metabolite to the difference between the two plant groups. The color of the bar indicates the significance of the difference in metabolite levels between the two groups, that is, the *P* value. One asterisk (*) represents $P<0.05$, two (**) represent $P<0.01$, and three (***) represent $P<0.001$

The analyzed data support that the identified metabolites drive the assembly of the healthy endophytic microbiota and directly influence plant health. However, further research is required to define whether the metabolites come from the plants or their microbiota.

Discussion

We performed untargeted metabolomic and metataxonomic analyses based on 16S and internal transcribed spacer (ITS) rRNA gene amplicons to identify metabolome-driven microbiome changes associated with ginger plant health and rhizome rot disease. The key findings of our study present a comprehensive overview of the biodiversity of soilborne and endophytic microbiota in both healthy and diseased ginger plant environments. This highlights the bacterial and fungal microbes that may contribute to plant health, as well as the specific metabolites that play a role in healthy microbial assembly and overall plant health.

Members of Proteobacteria, such as Burkholderiales, Rhizobiales, and Enterobacteriales, were the predominant members of the global bacterial community in ginger plants. Actinobacteria, Bacteroidetes, and Firmicutes followed in abundance. This differs from the top four reported for natural ecosystems [46]. However, it has been reported that host species and soil type [47], crop rotation [48], and environmental conditions like temperature, relative humidity, and pH [49] cooperatively modulated microbiome assembly.

The global fungal assemblage of ginger plants was dominated by members of Ascomycota, with *Hypocreale*, *Glomerellales*, *Pezizales*, and *Sordariales* being the most abundant. The kingdom of fungi, including true fungi (Fungi) and fungus-like organisms (e.g., Oomycota), is the second largest group of organisms, with an estimated 2.2 to 3.8 million species worldwide [50]. Surprisingly, approximately 60% of the fungal taxa are classified as unclassified_k_Fungi, indicating a need for further analysis. More comprehensive information on the complete ITS sequence of these microbes in databases is required to address this issue.

Several agents can cause soft rot (rhizome rot) in ginger, but generally, the "bad guys" are fungi from the *Fusarium* [25] and *Pythium* [28] genera. Interestingly, despite sequencing, these soilborne fungus was rarely detected. Previous studies also failed to identify *Pythium*, possibly due to the limitations of the ITS region [51]. The ITS3/ITS4 primer set effectively analyzed soil fungal biodiversity in various soil types [52]. DNA metabarcoding targeting the ITS region revealed the widespread presence of potentially plant-pathogenic *Phytophthora* and *Pythium* species in rhizospheric soil associated with internationally transported plants [53]. However, the ITS region lacks sufficient resolution for distinguishing closely related species of indoor and foodborne molds, plant pathogens, or other fungi, for which secondary barcode markers have been suggested [50]. We identified these species using ITS3/ITS4 barcoding, except for oomycotes in the ginger ecosystem.

Further research is required to understand better the absence of such globally widespread fungal species in ginger ecosystems. However, manure application promotes saprotrophic fungi while suppressing potential soilborne pathogenic fungi [54]. *Pectobacterium* spp. use synchronized production of plant cell wall-degrading enzymes (PCWDEs) as their primary virulence attribute. These bacteria enter the host through stomatal openings and wounds, colonizing xylem vessels, parenchyma, and protoxylem cells [55].

At the genus level, 16S rRNA gene sequencing revealed *Flavobacterium*, *Acidovorax*, *Sphingomonas*, *Methylobacterium-Methylorubrum*, and *Bacillus* as the most abundant genera. These genera were shared across all the ginger microbial niches. Research on the assembly of the bacterial microbiota in the endosphere and rhizosphere of rice plants has identified *Acidovorax*, *Sphingomonas*, *Bacillus*, and *Pseudomonas* as members of the core generalist microbiota [56].

The diversity and species richness of the ginger microbiota narrowed from the soil as a "seed bank" to the plant organs, which suggest that the plants actively filtered the microbiota composition. Rhizome rot disease causes a significant change in the microbial community of ginger plants, especially in terms of microbial diversity. This change may be due to the plant's reduced ability to filter organisms as the disease progresses.

The microbial structure detected in the rhizomes of both healthy and diseased plants revealed that specialist microbes did not cause rhizome rot. Instead, an imbalance caused by satellite [57] microbes like *Pectobacterium* was primarily detected in the stems and rhizomes of diseased plants. Saprotrophic fungi often take advantage of weakened diseased plants by colonizing their roots and rhizomes, while healthy plants maintain them in the soil. The presence of these fungi suggests that the cause of rhizome root disease is a necrotrophic pathogen that kills plant cells to feed on dead tissues and encourages the presence of other saprotrophs [58]. Most plant pathogens are mainly found in the rhizomes of diseased plants, although they have been discovered in all plant organs. This aligns with disease symptoms that spread to the entire plant.

Healthy plants harbor a more significant number and variety of bacterial microbes compared to diseased plants, while rhizome rot increases the diversity of

fungal microbes. Changes in microbiota composition have been associated with immune suppression during pathogen infections. In the leaves of *Arabidopsis* immune-compromised mutants, the Shannon diversity index and the relative abundance of Firmicutes were significantly decreased, while Proteobacteria were more prevalent [59]. These findings are similar to some aspects of dysbiosis in human inflammatory bowel disease [60].

The higher diversity of endophytic bacteria in healthy plants is likely due to the abundance of beneficial bacteria. Conversely, diseased plants have a more diverse range of bacteria in the rhizosphere, possibly due to decaying roots providing nutrients for soil organisms. In a study involving tobacco plants infected with *Ralstonia solanacearum* wilt, researchers found that healthy plants had a greater diversity of microorganisms than diseased plants. They observed increased levels of certain bacteria that promote plant growth and suppress diseases [61]. Similarly, healthy mulberry plant samples exhibited greater diversity of beneficial bacteria compared to those infected with bacterial wilt [62].

Among the bacterial species important in keeping plants healthy, *Q. granulorum* is capable of nitrification, denitrification, and polyphosphate accumulation [63]. *M. komagatae* was reported to be a potential biostimulator against fungal pathogens of ginger [64]. *Sphingomonas* species have variable functions, ranging from the remediation of environmental pollution to the production of highly beneficial plant growth regulators [65], and some strains are also involved in nitrogen fixation [59]. *Bacillus* spp. serves multiple ecological functions, from soil nutrient cycling to inducing plant growth and stress tolerance [66].

In contrast, among the bacteria that were associated with the disease, only a *P. brasiliense* strain TS20HJ1 was isolated from ginger rhizome and shown to cause soft rot symptoms [25]. *A. faecalis* is a heterotrophic nitrifying bacterium that oxidizes ammonia and generates nitrite and nitrate [67], and *K. aerogenes* significantly enhances the production of plant biomass and plant secondary metabolites [68].

In relation to the fungi that were enriched in the disease-suppressive soil, *Pseudaleuria* had been negatively correlated with the disease severity index of *Pisum sativum* L. [69] and its abundance was favored by the application of manure rather than mineral fertilization [70]. A high abundance of *Pseudogymnoascus* in the rhizosphere contributes to the nutrient cycling and helps crops better adapt to the environment [57]; these fungi are antagonistic to potato scab pathogens [71]. *Gymnoascus* spp. can also antagonistically affect pathogens and promote plant growth [72]. *Mortierella* species promote plant growth and have beneficial effects by modifying the soil microbiological composition [73].

Interestingly, *P. cucumerina* served as a biomarker for the endophyte microbiota of diseased plants and soil. The *Plectosphaerellaceae* species *G. piscis* and *P. cucumerina* have been previously described as pathogens of essential crop plants [74, 75]. However, to our knowledge, these fungi have not been previously reported as pathogens of ginger.

Analysis of the correlation between microbial communities and metabolomes remains scarce. Specific metabolites can attract beneficial microbes that defend against pathogens, while others exclude specific species from the microbial community [14]. The results revealed a metabolome-associated deterministic assembly process in the microbiota of the various microbial niches of ginger plants. The highest number of differentially accumulated metabolites between healthy and diseased plants was found in the plant compartments that hosted a greater diversity of fungal microbes, i.e., rhizomes and roots.

Recent research on ginger has revealed detailed information about its over 60 bioactive compounds, including phenolic compounds, terpenes, polysaccharides, lipids, and dietary fibers [76–79]. Some compounds can attract beneficial microbes that protect the plant from pathogens, while others may harm the microbial community [13, 80]. Remarkably, our research has shown that lipids and lipid-like molecules are the most prevalent metabolites, among the more than 700 identified using untargeted metabolomics, that contribute to the health of ginger plants, particularly in preventing rhizome rot disease. Lipids, a principal constituent of cell membranes, act as the interface and mediate cell signaling pathways after microbe recognition, allowing advantageous resource exchange or inhibiting interaction through downstream signaling cascades [81, 82]. Furthermore, when plants are exposed to necrotrophic pathogens such as *Pectobacterium* species, their immune responses often involve oxylipins, signaling molecules derived from oxygenated fatty acids and related metabolites [83].

We hypothesized that the metabolites exhibiting more variability in abundance in healthy or diseased ginger plants may be closely associated with the plants' responses to disease onset. Interestingly, the organoxygen compound 6-({[3,4-dihydroxy-4-(hydroxymethyl) oxolan-2-yl]oxy}methyl)oxane-2,3,4,5-tetrol was the only overexpressed metabolite in all the vegetative organs of healthy plants related to those of diseased plants, but its role in plant protection needs to be elucidated.

The levels of numerous rice amino acids increased in response to high saline–alkali stress, with threoninylproline showing the most significant increase [84]. Glu-Val is a dipeptide composed of L-valine and L-glutamic acid residues. Amino acids and their metabolites have

also been observed to stimulate the immune system in plants. Treating rice roots with Glu, and to a lesser extent Val, led to systemic disease resistance against rice blast (*Magnaporthe oryzae*) in leaves.

Niacinamide derivatives have been synthesized, and their fungicidal activity has been demonstrated [85]. Arachidonic acid (AA), a microbe-associated molecular pattern (MAMP) not commonly found in plants, is a potent elicitor of plant defense. Treating roots with AA-protected pepper and tomato seedlings from root and crown rot caused by *Phytophthora capsici*, leading to lignification at sites of attempted infection [86]. A relative of the ginger health biomarker *M. polycephala*, *M. alpina* has also been identified as an attractive AA producer [87]. In transgenic *A. thaliana* plants producing arachidonic acid, levels of jasmonic acid were increased, while levels of salicylic acid were decreased [88].

4-Methylene-L-glutamine is a nonproteinogenic L-alpha-amino acid that has been implicated in the transport of nitrogen [89]; coincidentally, the most prominent features of bacterial dysbiosis related to rhizome rot are related to the nitrogen cycle. Asparagine accumulation as part of nitrogen remobilization has been recorded in response to diverse abiotic and biotic stressors, such as disease and mineral limitation, as an adaptative process [90]. These changes in amino acids may be the result of disease in niches of ginger plants, although members of the *Rhizobium* complex of nitrogen-fixing bacteria were also enriched in the rhizome, stem, and leaves of diseased ginger plants.

Palmitoleamide is a primary fatty amide. A crude extract from the endophytic fungus *Botryodiplodia theobromae* containing fatty acid amides was observed to be broadly antimicrobial [91]. This metabolite was accumulated in stems of diseased ginger plants and showed a negative effect on microbes of the plant growth-promoting bacterial genus *Methylobacterium–Methylorubrum*. 4-Hydroxy nonenal alkyne, primarily detected in leaves of diseased ginger plants, is a significant aldehyde produced during the lipid peroxidation of ω-6 polyunsaturated fatty acids [92, 93].

Despite the limitations of this study, particularly concerning abundance thresholds for microbe inclusion, which need to be proven by culturomics methods, these limitations do not negatively impact the conclusions. Our findings provide a foundation for achieving disease suppression via modification of the metabolome-associated microbiome and have implications for further exploring pathogens, biocontrol agents, and plant growth promoters associated with economically important crop. Most microbial species and metabolites have not been previously identified in ginger plants. The assembly of the microbiota rather than the occurrence of a particular microbe drove plant health.

Supplementary Information

The online version contains supplementary material available at https://doi.org/10.1186/s40168-024-01885-y.

Supplementary Material 1: Supplementary Table 1. OTU table for the archaeal/bacterial ginger microbiome. The total number of OTUs in each of the three composite biological replicates is shown. HPBS: healthy plant bulk soil, DPBS: diseased plant bulk soil, HPRhS: healthy plant rhizosphere soil, DPRhS: diseased plant rhizosphere soil, HPRh: healthy plant rhizome, DPRh: diseased plant rhizome, HPR: healthy plant root, DPR: diseased plant root, HPS: healthy plant stem, DPS: diseased plant stem, HPL: healthy plant leaf, DPL: diseased plant leaf.

Supplementary Material 2: Supplementary Table 2. OTU table for the fungal ginger microbiome. The total number of OTUs in each of the three composite biological replicates is shown. HPBS: healthy plant bulk soil, DPBS: diseased plant bulk soil, HPRhS: healthy plant rhizosphere soil, DPRhS: diseased plant rhizosphere soil, HPRh: healthy plant rhizome, DPRh: diseased plant rhizome, HPR: healthy plant root, DPR: diseased plant root, HPS: healthy plant stem, DPS: diseased plant stem, HPL: healthy plant leaf, DPL: diseased plant leaf.

Supplementary Material 3: Supplementary Table 3. Core and specialists bacterial and fungal microbes. HPBS: healthy plant bulk soil, DPBS: diseased plant bulk soil, HPRhS: healthy plant rhizosphere soil, DPRhS: diseased plant rhizosphere soil, HPRh: healthy plant rhizome, DPRh: diseased plant rhizome, HPR: healthy plant root, DPR: diseased plant root, HPS: healthy plant stem, DPS: diseased plant stem, HPL: healthy plant leaf, DPL: diseased plant leaf.

Supplementary Material 4: Supplementary Table 4. Bacterial functional assemblages based on FAPROTAX analysis. The values are the average of three composite biological replicates (mean), sd is the standard variation in the mean for each microbial niche. Testing for significance was performed using a Kruskal–Wallis rank sum test.

Supplementary Material 5: Supplementary Table 5. Identification of specific ecological categories of fungi through FUNGuild functional classification. The values are the average of three composite biological replicates. HPBS: healthy plant bulk soil, DPBS: diseased plant bulk soil, HPRhS: healthy plant rhizosphere soil, DPRhS: diseased plant rhizosphere soil, HPRh: healthy plant rhizome, DPRh: diseased plant rhizome, HPR: healthy plant root, DPR: diseased plant root, HPS: healthy plant stem, DPS: diseased plant stem, HPL: healthy plant leaf, DPL: diseased plant leaf.

Supplementary Material 6: Supplementary Table 6. Co-occurrence Network statistics for bacterial microbiota in healthy plants. Nodes represent microbial genera, and edges represent the statistically significant associations between nodes. Connections were drawn between significantly correlated nodes ($P < 0.05$ and Spearman's $r > 0.96$; Spearman's rank correlation test).

Supplementary Material 7: Supplementary Table 7. Co-occurrence Network statistics for bacterial microbiota in diseased plants. Nodes represent microbial genera, and edges represent the statistically significant associations between nodes. Connections were drawn between significantly correlated nodes ($P < 0.05$ and Spearman's$r > 0.96$; Spearman's rank correlation test).

Supplementary Material 8: Supplementary Table 8. Co-occurrence Network statistics for fungal microbiota in healthy ginger plants. Nodes represent microbial genera, and edges represent the statistically significant associations between nodes. Connections were drawn between significantly correlated nodes ($P < 0.05$ and Spearman's $r > 0.96$; Spearman's rank correlation test).

Supplementary Material 9: Supplementary Table 9.Co-occurrence Network statistics for fungal microbiota in diseased ginger plants. Nodes represent microbial genera, and edges represent the statistically significant associations between nodes. Connections were drawn between significantly correlated nodes ($P < 0.05$ and Spearman's $r > 0.96$; Spearman's rank correlation test).

Supplementary Material 10: Supplementary Table 10. Overview of metabolite information. ID: In the data matrix identified by searching the mass

spectrometry library, the number of each identified ion peak is randomly assigned according to different ion modes; Metabolite: the name of the metabolite identified in this project; Metab ID: In the cloud platform analysis, the number of each identified ion peak is randomly assigned; Library ID: the metabolite is found in the corresponding accession number of the search database; KEGG compound ID: the accession number of the KEGG database; M/Z or Quantum Mass: mass-charge ratio; Retention time: refers to the retention time of charged ions in chromatography; Mode: ion detection mode, including positive ion and negative ion mode; Adducts: adduct ionic mode, refers to the covalent bond between metabolites and cellular macromolecules; Formula: chemical formula of metabolites; Fragmentation score: Metlin database search score; Theoretical fragmentation score: HMDB database search score; Mass error: mass deviation (ppm)); CAS ID: chemical substance registration number; RSD: relative standard deviation of quality control samples.

Supplementary Material 11: Supplementary Table 11. Niche-specific expression of metabolites associated with plant health. ID: In the data matrix obtained by the mass spectrometry search database, each ion peak is randomly numbered according to different ion modes; metabolite: metabolite detected; VIP_value represents the contribution value of the metabolite to the difference between the two niches of healthy and diseased plants; VIP: The higher the value, the more significant the difference between the two groups of metabolites; *P*_value: indicates the significance of the difference between the two groups of samples for the given metabolite; HP: indicates the relative expression level of the metabolite in the healthy plant samples; DP: indicates the relative expression level of the metabolite in the samples from the diseased plants.

Supplementary Material 12: Supplementary Fig. 1. Shannon rarefaction curves of the archaeal/bacterial (A) and fungal (B) community groups at the OTU level. The rarefaction curve was calculated by randomly resampling each sample several times and then plotting the rarefied number of OTUs defined at a 97% sequence similarity threshold relative to the number of samples. The abscissa represents the amount of sequencing data randomly sampled, and the ordinate represents the diversity index (Shannon index) at the OTU level. Rank abundance analysis of the archaeal/bacterial (C) and fungal (D) community groups at the OTU level. The abscissa represents the rank of the OTU, and the ordinate represents the relative percentage of the abundance of the OTU. The position on the abscissa of the open end of the sample curve corresponds to the number of OTUs in the sample.

Supplementary Material 13: Supplementary Fig. 2. Co-occurrence network analysis of the microbial community associated with the health of the ginger plant. Co-occurrence of bacterial (A) and fungal genera (B) in health (S1) and diseased (S1D) ginger plants based on relative abundance. Different colors represent microbial genera associated with healthy (blue) and diseased (red) plants; black is the keystone core genera. Intra-kingdom network analysis of the ginger microbiome is conducted based on correlation analysis of taxonomic profiles in healthy (C for bacteria and E for fungi) and diseased (D for bacteria and F for fungi) ginger plants. Nodes represent microbial genera, and edges represent the statistically significant associations between nodes. Connections were drawn between significantly correlated nodes ($P < 0.05$ and Spearman's $r > 0.96$; Spearman's rank correlation test). The red edges are indicators of co-occurrence (positive), and the green edges are indicators of mutual exclusion (negative) correlations. Hub microbes for each network are ranked according to the number of connections in the network.

Supplementary Material 14: Supplementary Fig. 3. Quality control (QC) metabolomic sample evaluation. By calculating the relative standard deviation (RSD) value of each variable in the QC sample, variables whose RSD exceeds the threshold are eliminated, and variables with RSD ≤ 30% are retained. The abscissa is the RSD value (%), i.e., the standard deviation/mean value, and the ordinate is the ratio of ion peaks. The dotted line indicates the value before preprocessing, while the solid line shows the results after preprocessing.

Authors' contributions
R.S.B., W.W. and W.H. conceived the study. W.W., N.P.G., J.L., and P.R. performed the experiments and analyzed the data. W.H., X.W., H.L. and R.S.B. supervised and provided the suggestion of the research work. R.S.B. and O.B.H. wrote the manuscript. All authors contributed to the article and approved the submitted version.

Funding
This study was jointly supported by the Shandong Province Double Hundred Talent Plan No. WSG20200001.

Availability of data and materials
Original contributions presented in the study are included in the manuscript. All the fastq files resulting from the Illumina platform are publicly available in the Sequence Read Archive (SRA) of the National Center for Biotechnology Information (NCBI) database (bacteria 16S rRNA gene: accession no. PRJNA1035274; fungal ITS: accession no. PRJNA1035275). Metabolomic data is available at BIG Submission (BIG SUB, bioproject PRJCA023529, https://ngdc.cncb.ac.cn/omix/release/OMIX005846, OMIX ID: OMIX005846). The unrarified OTU table for bacterial and fungal microbes, statistical analyses, and overview of metabolite information have all been included as Additional files.

Declarations

Ethics approval and consent to participate
Not applicable.

Consent for publication
Not applicable.

Competing interests
The authors declare no competing interests.

Author details
[1]School of Biological Science and Technology, University of Jinan, No. 336, West Road of Nan Xinzhuang, Jinan, Shandong 250022, People's Republic of China. [2]Joint R&D Center of Biotechnology, RETDA, Yota Bio-Engineering Co., Ltd., 99 Shenzhen Road, Rizhao, Shandong 276826, People's Republic of China.

Received: 25 January 2024 Accepted: 27 July 2024
Published online: 07 September 2024

References

1. Johnson JS, Spakowicz DJ, Hong BY, Petersen LM, Demkowicz P, Chen L, et al. Evaluation of 16S rRNA gene sequencing for species and strain-level microbiome analysis. Nat Commun. 2019;10(1):5029.
2. Pang Z, Chen J, Wang T, Gao C, Li Z, Guo L, et al. Linking plant secondary metabolites and plant microbiomes: a review. Front Plant Sci. 2021;12:621276.
3. Hildebrand F, Tedersoo L, Mander Ü. Structure and function of the soil microbiome underlying N_2O emissions from global wetlands. Nat Commun. 2022;13(1):1430.
4. DiLegge MJ, Manter DK, Vivanco JM. Soil microbiome disruption reveals specific and general plant-bacterial relationships in three agroecosystem soils. PLoS ONE. 2022;17(11): e0277529.
5. Schlatter D, Kinkel L, Thomashow L, Weller D, Paulitz T. Disease suppressive soils: new insights from the soil microbiome. Phytopathology. 2017;107(11):1284–97.
6. Philippot L, Raaijmakers JM, Lemanceau P, van der Putten WH. Going back to the roots: the microbial ecology of the rhizosphere. Nat Rev Microbiol. 2013;11(11):789–99.
7. Liu H, Carvalhais LC, Schenk PM, Dennis PG. Effects of jasmonic acid signalling on the wheat microbiome differ between body sites. Sci Rep. 2017;7:41766.
8. Haney C, Samuel B, Bush J, Ausubel FM. Associations with rhizosphere bacteria can confer an adaptive advantage to plants. Nat Plants. 2015;1:15051.
9. Ling N, Wang T, Kuzyakov Y. Rhizosphere bacteriome structure and functions. Nat Commun. 2022;13:836.
10. Beckers B, Op De Beeck M, Thijs S, Truyens S, Weyens N, Boerjan W, & Vangronsveld J. Performance of 16s rDNA primer pairs in the study of rhizosphere and endosphere bacterial microbiomes in metabarcoding studies. Front Microbiol. 2016;7:650.

11. Kudjordjie EN, Hooshmand K, Sapkota R, Darbani B, Fomsgaard IS, Nicolaisen M. *Fusarium oxysporum* disrupts microbiome-metabolome networks in *Arabidopsis thaliana* roots. Microbiol Spectrum. 2022;10(4): e0122622.
12. Carrión VJ, Perez-Jaramillo J, Cordovez V, Tracanna, V, de Hollander, M, Ruiz-Bucket al. Pathogen-induced activation of disease-suppressive functions in the endophytic root microbiome. Science. 2019;366(6465):606–12.
13. Yuan J, Zhao J, Wen T, et al. Root exudates drive the soil-borne legacy of aboveground pathogen infection. Microbiome. 2018;6:156.
14. Howe A, Stopnisek N, Dooley SK, et al. Seasonal activities of the phyllosphere microbiome of perennial crops. Nat Commun. 2023;14:1039.
15. Meyer KM, Porch R, Muscettola IE, Vasconcelos ALS, Sherman JK, Metcalf CJE, et al. Plant neighborhood shapes diversity and reduces interspecific variation of the phyllosphere microbiome. ISME J. 2022;16(5):1376–87.
16. Gao M, Xiong C, Gao C, Tsui CKM, Wang MM, et al. Disease-induced changes in plant microbiome assembly and functional adaptation. Microbiome. 2021;9(1):187.
17. Korenblum E, Dong Y, Szymanski J, Panda S, Jozwiak A, Massalha H, et al. Rhizosphere microbiome mediates systemic root metabolite exudation by root-to-root signaling. Proc Natl Acad Sci USA. 2020;117(7):3874–83.
18. Seybold H, Demetrowitsch TJ, Hassani MA, Szymczak S, Reim E, Haueisen et al. A fungal pathogen induces systemic susceptibility and systemic shifts in wheat metabolome and microbiome composition. Nat Commun. 2020;11(1):1910.
19. Chen X, Marszałkowska M, Reinhold-Hurek B. Jasmonic acid, not salicyclic acid restricts endophytic root colonization of rice. Front Plant Sci. 2020;10:1758.
20. Chen Y, Bonkowski M, Shen Y, Griffiths BS, Jiang Y, Wang X, Sun B. Root ethylene mediates rhizosphere microbial community reconstruction when chemically detecting cyanide produced by neighbouring plants. Microbiome. 2020;8:4.
21. Yang L, Zhou M, Zu M, Yuan Y. Comprehensive microbiome and metabolome analyses reveal the medicinal components of *Paeonia lactiflora*. Plants (Basel, Switzerland). 2023;12(8):1612.
22. Li H, Shi H, Xu P, Yu D. Metabolomics and microbiome reveal potential root microbiota affecting the alkaloidal metabolome in *Aconitum vilmorinianum* Kom. BMC Microbiol. 2022;22(1):70.
23. Liu Y, Wu L, Wu X, Li H, Liao Q, Zhang X et al. Analysis of microbial diversity in soil under ginger cultivation. Scientifica. 2017;8256865
24. Chawla S, Rafie RA, Likins TM, Ndegwa E, Ren S & Mersha Z. First report of Fusarium yellows and rhizome rot caused by *Fusarium oxysporum* f. sp. *zingiberi* on ginger in the continental United States. Plant Dis. 2021;https://doi.org/10.1094/PDIS-03-21-0658-PDN.
25. Wang J, Lu Y, Han W, Fu L, Han X, Zhu J & Zhang S. First report of rhizome rot caused by *Pectobacterium brasiliense* on ginger in China. Plant Dis. 2022:PDIS10212324PDN.
26. Peng Q, Yuan Y, Gao M. *Bacillus pumilus*, a novel ginger rhizome rot pathogen in China. Plant Dis. 2013;97(10):1308–15.
27. Stirling GR, Turaganivalu U, Stirling AM, Lomavatu MF, Smith MK. Rhizome rot of ginger (*Zingiber officinale*) caused by *Pythium myriotylum* in Fiji and Australia. Australas Plant Pathol. 2009;38:453–60.
28. Liu J, Zhao Z & Wang C. First report of rhizome rot on ginger (*Zingiber officinale*) caused by *Enterobacter cloacae* in Shandong Province, China. Plant Dis. 2020:https://doi.org/10.1094/PDIS-05-20-1108-PDN.
29. Agler MT, Ruhe J, Kroll S, Morhenn C, Kim ST, Weigel D, Kemen EM. Microbial hub taxa link host and abiotic factors to plant microbiome variation. PLoS Biol. 2016;14(1): e1002352.
30. Li J, Zhang GZ, Li X, Wang Y, Wang FZ, Li XM. Seasonal change in response of stomatal conductance to vapor pressure deficit and three phytohormones in three tree species. Plant Signal Behav. 2019;14(12): 682341.
31. Liu S, Yang G, Wu F, Ge Y, Liu F, Pu C, et al. Traditional Chinese medicine residues promote the growth and quality of *Salvia miltiorrhiza* Bunge by improving soil health under continuous monoculture. Front Plant Sci. 2023;14:1112382.
32. Schlaeppi K, Bulgarelli D. The plant microbiome at work. Mol Plant Microbe Interact. 2015;28(3):212–7.
33. Li R, Duan W, Ran Z, Chen X, Yu H, Fang L. et al. Diversity and correlation analysis of endophytes and metabolites of *Panax quinquefolius* L. in various tissues. BMC Plant Biol. 2023;23:275.
34. White TJ, Bruns TD, Lee SB, Taylor JW. Amplification and direct sequencing of fungal ribosomal RNA genes for phylogenetics. In: Innis MA, Gelfand DH, Sninsky JJ, White TJ, editors. PCR protocols: a guide to methods and applications. United States: Academic Press; 1990. p. 315–22.
35. Op De Beeck M, Lievens B, Busschaer P, Declerck S, Vangronsveld J & Colpaert JV. Comparison and validation of some ITS primer pairs useful for fungal metabarcoding studies. PloS One. 2014;9(6):e97629.
36. Ren Y, Yu G, Shi CP, Liu L, Guo Q, Han C et al. Majorbio Cloud: a one-stop, comprehensive bioinformatic platform for multiomics analyses. iMeta. 2022;1:e12.
37. Caporaso JG, Kuczynski J, Stombaugh J, Bittinger K, Bushman FD, Costello EK, et al. QIIME allows analysis of high-throughput community sequencing data. Nat Methods. 2010;7(5):335–6.
38. Edgar RC. Search and clustering orders of magnitude faster than BLAST. Bioinformatics (Oxford, England). 2010;26(19):2460–1.
39. Edgar RC. UPARSE: highly accurate OTU sequences from microbial amplicon reads. Nat Methods. 2013;10:996–8.
40. Wei F, Zhao L, Xu X, Feng H, Shi Y, Deakin G. Cultivar-dependent variation of the cotton rhizosphere and endosphere microbiome under field conditions. Front Plant Sci. 2019;10:1659.
41. Lemos LN, Fulthorpe RR, Triplett EW, Roesch LF. Rethinking microbial diversity analysis in the high throughput sequencing era. J Microbiol Methods. 2011;86:42–51.
42. Kembel SW, Cowan PD, Helmus MR, Cornwell WK, Morlon H, Ackerly DD, et al. Picante: R tools for integrating phylogenies and ecology. Bioinformatics. 2010;26:1463–4.
43. Louca S, Parfrey LW, Doebeli M. Decoupling function and taxonomy in the global ocean microbiome. Science (New, NY). 2016;353(6305):1272–7.
44. Nguyen NH, Song Z, Bates ST, Branco S, Tedersoo L, Menke J, et al. FUNGuild: an open annotation tool for parsing fungal community datasets by ecological guild. Fungal Ecol. 2016;20:241–8.
45. Chong J, Xia J. Computational approaches for integrative analysis of the metabolome and microbiome. Metabolites. 2017;7(4):62.
46. Lauber CL, Hamady M, Knight R, Fierer N. Pyrosequencing-based assessment of soil pH as a predictor of soil bacterial community structure at the continental scale. Appl Environ Microbiol. 2009;75(15):5111–20.
47. Liu F, Hewezi T, Lebeis SL, Pantalone V, Grewal PS, Staton ME. Soil indigenous microbiome and plant genotypes cooperatively modify soybean rhizosphere microbiome assembly. BMC Microbiol. 2019;19(1):201.
48. Zhou Y, Yang Z, Liu J, Li X, Wang X, Dai C. et al. Crop rotation and native microbiome inoculation restore soil capacity to suppress a root disease. Nat Commun. 2023;14:8126.
49. Zhang Y, Su M, Wu F, Gu JD, Li J, He D, Guo Q, Cui H, Zhang Q, Feng H. Diversity and composition of culturable microorganisms and their biodeterioration potentials in the sandstone of Beishiku Temple, China. Microorganisms. 2023;11(2):429.
50. Lücking R, Aime MC, Robbertse B, Miller AN, Ariyawansa HA, Aoki T, et al. Unambiguous identification of fungi: where do we stand and how accurate and precise is fungal DNA barcoding? IMA fungus. 2020;11:14.
51. Wang CW, Michelle Wong JW, Yeh SS, Eric Hsieh Y, Tseng CH, et al. Soil bacterial community may offer solutions for ginger cultivation. Microbiol Spectrum. 2022;10(5): e0180322.
52. Yu Y, Yang Q, Petropoulos E, Zhu T. ITS3/ITS4 outperforms other ITS region and 18S rRNA gene primer sets for amplicon sequencing of soil fungi. Eur J Soil Sci. 2022;73(6): e13329.
53. Rossmann S, Lysøe E, Skogen M, Talgø V, Brurberg MB. DNA metabarcoding reveals broad presence of plant pathogenic oomycetes in soil from internationally traded plants. Front Microbiol. 2021;12: 637068.
54. Ye G, Banerjee S, He J, Fan J, Wang Z, Wei X, et al. Manure application increases microbiome complexity in soil aggregate fractions: results of an 18-year field experiment. Agr Ecosyst Environ. 2021;307: 107249.
55. Charkowski AO. The changing face of bacterial soft-rot diseases. Annu Rev Phytopathol. 2018;56:269–88.
56. Guo J, Ling N, Li Y, Li K, Ning H, Shen Q, et al. Seed-borne, endospheric and rhizospheric core microbiota as predictors of plant functional traits across rice cultivars are dominated by deterministic processes. New phytol. 2021;230(5):2047–60.
57. Sahu KP, Kumar A, Sakthivel K, Reddy B, Kumar M, Patel A, et al. Deciphering core phyllomicrobiome assemblage on rice genotypes grown in contrasting agroclimatic zones: implications for phyllomicrobiome engineering against blast disease. Environ Microbiome. 2022;17(1):28.

58. Chowdhury S, Basu A, Kundu S. Biotrophy-necrotrophy switch in pathogen evoke differential response in resistant and susceptible sesame involving multiple signaling pathways at different phases. Sci Rep. 2017;7:17251.
59. Chen T, Nomura K, Wang X, Sohrabi R, Xu J, Yao L, et al. A plant genetic network for preventing dysbiosis in the phyllosphere. Nature. 2020;580:653–7.
60. Paasch BC, He SY. Toward understanding microbiota homeostasis in the plant kingdom. PLoS pathogens. 2021;17(4).
61. Ahmed W, Dai Z, Liu Q, Munir S, Yang J, Karunarathna SC, et al. Microbial cross-talk: dissecting the core microbiota associated with flue-cured tobacco (*Nicotiana tabacum*) plants under healthy and diseased state. Front Microbiol. 2022;13: 845310.
62. Yuan T, Qazi IH, Li J, Yang P, Yang H, Zhang X, et al. Analysis of changes in bacterial diversity in healthy and bacterial wilt mulberry samples using metagenomic sequencing and culture-dependent approaches. Front Plant Sci. 2023;14:1206691.
63. Maszenan AM, Tay JH, Schumann P, Jiang HL & Tay S T. *Quadrisphaera granulorum* gen. nov., sp. nov., a Gram-positive polyphosphate-accumulating coccus in tetrads or aggregates isolated from aerobic granules. International journal of systematic and evolutionary microbiology. 2005;55(Pt 5):1771–1777.
64. Vadivukkarasi P, Bhai RS. Phyllosphere-associated *Methylobacterium*: a potential biostimulant for ginger (*Zingiber officinale* Rosc.) cultivation. Arch Microbiol. 2020;202:369–375.
65. Asaf S, Numan M, Khan AL, Al-Harrasi A. *Sphingomonas*: from diversity and genomics to functional role in environmental remediation and plant growth. Crit Rev Biotechnol. 2020;40(2):138–52.
66. Katsenios N, Andreou V, Sparangis P, Djordjevic N, Giannoglou M, Chanioti S, et al. Assessment of plant growth promoting bacteria strains on growth, yield and quality of sweet corn. Sci Rep. 2022;12:11598.
67. Tsujino S, Dohra H, Fujiwara T. Gene expression analysis of Alcaligenes faecalis during induction of heterotrophic nitrification. Sci Rep. 2021;11:23105.
68. Shukla N, Singh D, Tripathi A, Kumari P, Gupta RK, Singh S, et al. Synergism of endophytic *Bacillus subtilis* and *Klebsiella aerogenes* modulates plant growth and bacoside biosynthesis in Bacopa monnieri. Front Plant Sci. 2022;13: 896856.
69. Xu LH, Ravnskov S, Larsen J, Nilson RH, Nicolaisen M. Soil fungal community structure along a soil health gradient in pea fields examined using deep amplicon sequencing. Soil Biol Biochem. 2012;46:26–32.
70. Xiang X, Liu J, Jie Z, Daming L, Changxu X, Kuzyakov Y. Divergence in fungal abundance and community structure between soils under long-term mineral and organic fertilization. Soil Tillage Res. 2020;196: 104491.
71. Tagawa M, Tamaki H, Manome A, Koyama O, Kamagata Y. Isolation and characterization of antagonistic fungi against potato scab pathogens from potato field soils. FEMS Microbiol Lett. 2010;305:136–42.
72. Zhou N, Zhang Y, Liu F, Cai L. Halophilic and thermotolerant Gymnoascus species from several special environments. China Mycologia. 2016;108(1):179–91.
73. Ozimek E, Hanaka A. Mortierella species as the plant growth-promoting fungi present in the agricultural soils. Agriculture. 2021;11:7.
74. Zhou Y, Zhao Z, Guo Q, Lei B. First report of wilt of sugar beet caused by *Gibellulopsis nigrescens* in the Xinjiang Region of China. Plant Dis. 2017;101:1318.
75. Li PL, Chai AL, Shi YX, Xie XW, Li BJ. First report of root rot caused by *Plectosphaerella cucumerina* on Cabbage in China. Mycobiology. 2017;45(2):110–3.
76. Jiang Y, Liao Q, Zou Y, Liu Y & Lan J. Transcriptome analysis reveals the genetic basis underlying the biosynthesis of volatile oil, gingerols, and diarylheptanoids in ginger (Zingiber officinale Rosc.). Bot Stud. 2017;58:41.
77. Mao QQ, Xu XY, Cao SY, Gan RY, Corke H, Beta T, Li HB. Bioactive compounds and bioactivities of ginger (*Zingiber officinale* Roscoe). Foods (Basel, Switzerland). 2019;8(6):185.
78. Li H-L, Wu L, Dong Z, Jiang Y, Jiang S, Xing H, et al. Haplotype-resolved genome of diploid ginger (Zingiber officinale) and its unique gingerol biosynthetic pathway. Horticulture Res. 2021;8:189.
79. Zhang W, Yang Y, Zhu X, Yang S, Liao X, Li H, et al. Integrated analyses of metabolomics and transcriptomics reveal the potential regulatory roles of long non-coding RNAs in gingerol biosynthesis. BMC Genom. 2023;24(1):490.
80. Luo L, Yang L, Yan Z, Jiang B-B, Li S, Huang H-C, et al. Ginsenosides in root exudates of Panax notoginseng drive the change of soil microbiota through carbon source different utilization. Plant Soil. 2020;455:139–53.
81. Mamode Cassim A, Gouguet P, Gronnier J, Laurent N, Germain V, Grison M, et al. Plant lipids: key players of plasma membrane organization and function. Prog Lipid Res. 2019;73:1–27.
82. Macabuhay A, Arsova B, Walker R, Johnson A, Watt M, Roessner U. Modulators or facilitators? Roles of lipids in plant root-microbe interactions. Trends Plant Sci. 2022;27(2):180–90.
83. Wasternack C, Feussner I. The oxylipin pathways: biochemistry and function. Annu Rev Plant Biol. 2018;69:363–86.
84. Qian G, Wang M, Wang X, Liu K, Li Y, Bu Y, Li L. Integrated transcriptome and metabolome analysis of rice leaves response to high saline-alkali stress. Int J Mol Sci. 2023;24(4):4062.
85. Zhou B, Ma C, Zheng C, Xia T, Ma B, Liu X. 3-Methylxanthine production through biodegradation of theobromine by *Aspergillus sydowii* PT-2. BMC Microbiol. 2020;20:26.
86. Dye SM, Bostock RM. Eicosapolyenoic fatty acids induce defense responses and resistance to *Phytophthora capsici* in tomato and pepper. Physiol Mol Plant Pathol. 2021;114: 101642.
87. Dedyukhina EG, Kamzolova SV, Vainshtein MB. Arachidonic acid as an elicitor of the plant defense response to phytopathogens. Chem Biol Technol Agric. 2014;1:18.
88. Savchenko T, Walley JW, Chehab EW, Xiao Y, Kaspi R, Pye MF, et al. Arachidonic acid: an evolutionarily conserved signaling molecule modulates plant stress signaling networks. Plant Cell. 2010;22(10):3193–205.
89. Hossain MI, Thomas AG, Mahdi F, Adam AT, Akins NS, Woodard MM, et al. An efficient synthetic route to l-γ-methyleneglutamine and its amide derivatives, and their selective anticancer activity. RSC Adv. 2021;11(13):7115–28.
90. Oddy J, Raffan S, Wilkinson MD, Stephen Elmore J, Hltford NG. Stress, nutrients and genotype: understanding and managing asparagine accumulation in wheat grain. CABI Agric Biosci. 2020;1:10.
91. Zaher AM, Moharram AM, Davis R, Panizzi P, Makboul MA & Calderón AI. Characterisation of the metabolites of an antibacterial endophyte *Botryodiplodia theobromae* Pat. of *Dracaena d*raco L. by LC–MS/MS. Nat Prod Res.2015;29:2275–81.
92. West JD, Marnett LJ. Endogenous reactive intermediates as modulators of cell signaling and cell death. Chem Res Toxicol. 2006;19(2):173–94.
93. Ge F, Yokochi N, Yoshikane Y, Ohnishi K, Yagi T. Gene identification and characterization of the pyridoxine degradative enzyme 4-pyridoxic acid dehydrogenase from the nitrogen-fixing symbiotic bacterium Mesorhizobium loti MAFF303099. J Biochem. 2008;143(5):603–9.

Publisher's Note